MASSACHUSETTS INSTITUTE OF TECHNOLOGY
DEPARTMENT OF EARTH AND PLANETARY SCIENCES
CAMBRIDGE, MASSACHUSETTS 02139

(4) FINAL TECHNICAL REPORT.

(6) FURTHER STUDIES OF TIDAL-CURRENT SAND WAVES.

(10) John B. Southard
Principal Investigator

(12) 49

(11) 15 Sep 81

(15) Office of Naval Research
Contract: N0014-78-C-0095

M.I.T. OSP No. 85979

SEP 15 1981

TABLE OF CONTENTS

Physiographic Setting

Middle Ground Shoal and Lucas Shoal extend nearly parallel to the axis of Vineyard Sound, Massachusetts (Fig. 1, 2). Their crests rise to depths of 7 to 8 m except at the northeastern end of Middle Ground Shoal, where water depths are only 2 to 3 m. Vineyard Sound is generally shallower and flatter-floored north of the shoal than south; to the south, depths increase to almost 30 m in a distance of less than 1 km from the axis of Middle Ground Shoal. The southeast flank of the shoal is much steeper than the northwest flank. The shoal is covered with fairly well rounded coarse sand (median size 0.87 mm), in contrast to the surrounding glacial till (Smith, 1969a). Median size is somewhat smaller, 0.2-0.5 mm, at the eastern tip of Middle Ground (Owen et al., 1967). Samples from sand-wave crests are substantially coarser than those from troughs.

The overall circulation in Vineyard Sound reflects a semi-diurnal tidal period. Ebb velocities (toward the southwest) reach 2.8 knots (1.42 m/sec) near Middle Ground Shoal, and are generally uniform across the width of the sound, whereas flood velocities (toward the northeast) reach 3.9 knots (1.98 m/sec) near the shoal, and show significantly higher velocities south of the shoal axis than to the north. Fig. 1 shows an example of tidal ellipses measured at two locations in Vineyard Sound by others. The net circulation in the sound is counter-clockwise, the northern side being dominated by ebb flow and the southern side by flood flow.

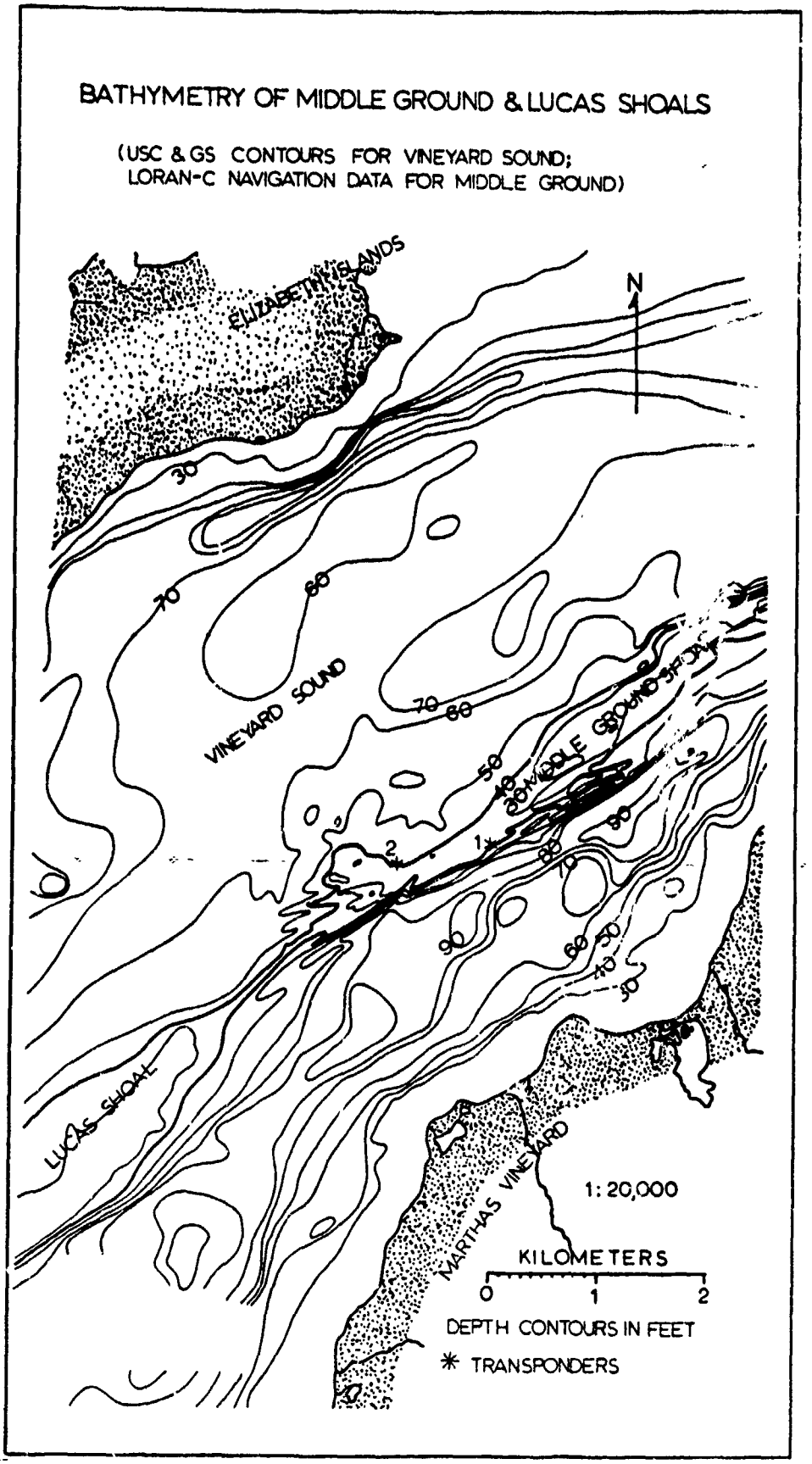

Figure 1. Chart of Vineyard Sound, Massachusetts, showing the general area of study on SW Middle Ground Shoal and typical tidal ellipses (contours from USCGGS chart).

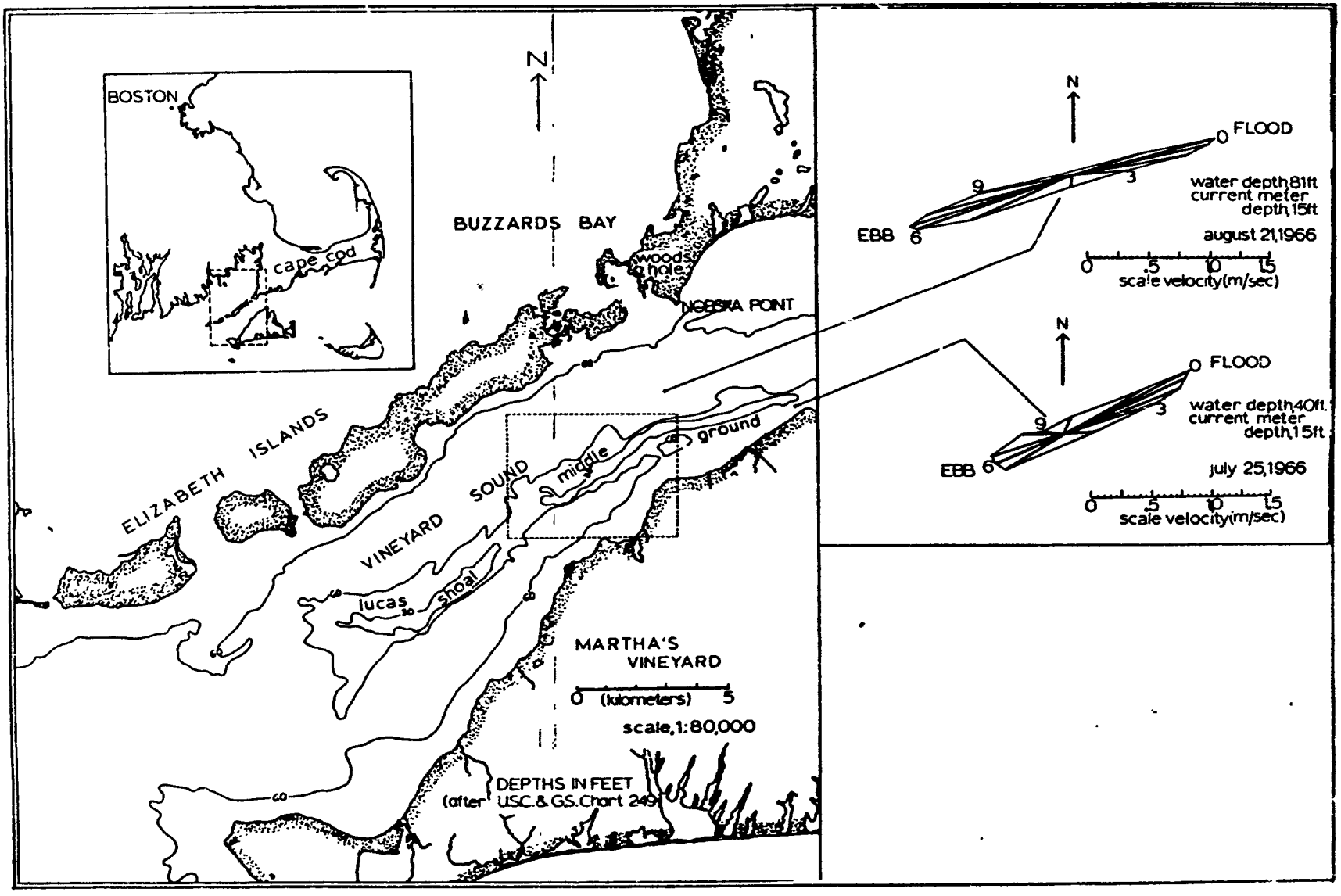

Figure 2. Detailed bathymetry of Vineyard Sound and the study area, based on Loran-C navigated surveys by Briggs (1979).

Navigation

Precision navigation and the ability to plot ship's position in real time were essential. Previous studies of sand-wave migration in other areas give yearly migration rates ranging from 0 to 150 meters per year (Jones et al., 1965; Salsman et al., 1966; Terwindt, 1971; Langhorne, 1973; Pasenau and Ulrich, 1974; Boothroyd and Hubbard, 1975; Dalrymple et al., 1975; Bokuniewicz et al., 1977; Dalrymple, 1977). Studies using more sophisticated navigation systems (Pasenau and Ulrich, 1974; Bokuniewicz et al., 1977) suggest a flexing mode of migration in which different segments of a sand wave advance at widely varying rates. Even if sand waves on Middle Ground Shoal migrated tens of meters per year, monthly mappings would need a precision of plus or minus a few meters to record month-to-month displacements. In addition, one's ability to place instrumentation at selected sites along a transect over a single sand wave in order to measure the velocity field over that wave requires positioning precision at least as good. Finally, in order to map completely a study area with nearly parallel track lines, real-time plots of ship position are needed during each survey.

To meet these requirements a TRANSNAV 6000 acoustic transponder navigation system (manufactured by Ocean Research Equipment, Inc., Falmouth, Massachusetts; ORE) was leased. For reasons of expense, a fixed baseline aligned NE-SW along the axis of the shoal and defined by a permanently emplaced acoustic transponder at each end was used in conjunction with a third transponder, positioned off the baseline and deployed only during each survey (Fig. 3).

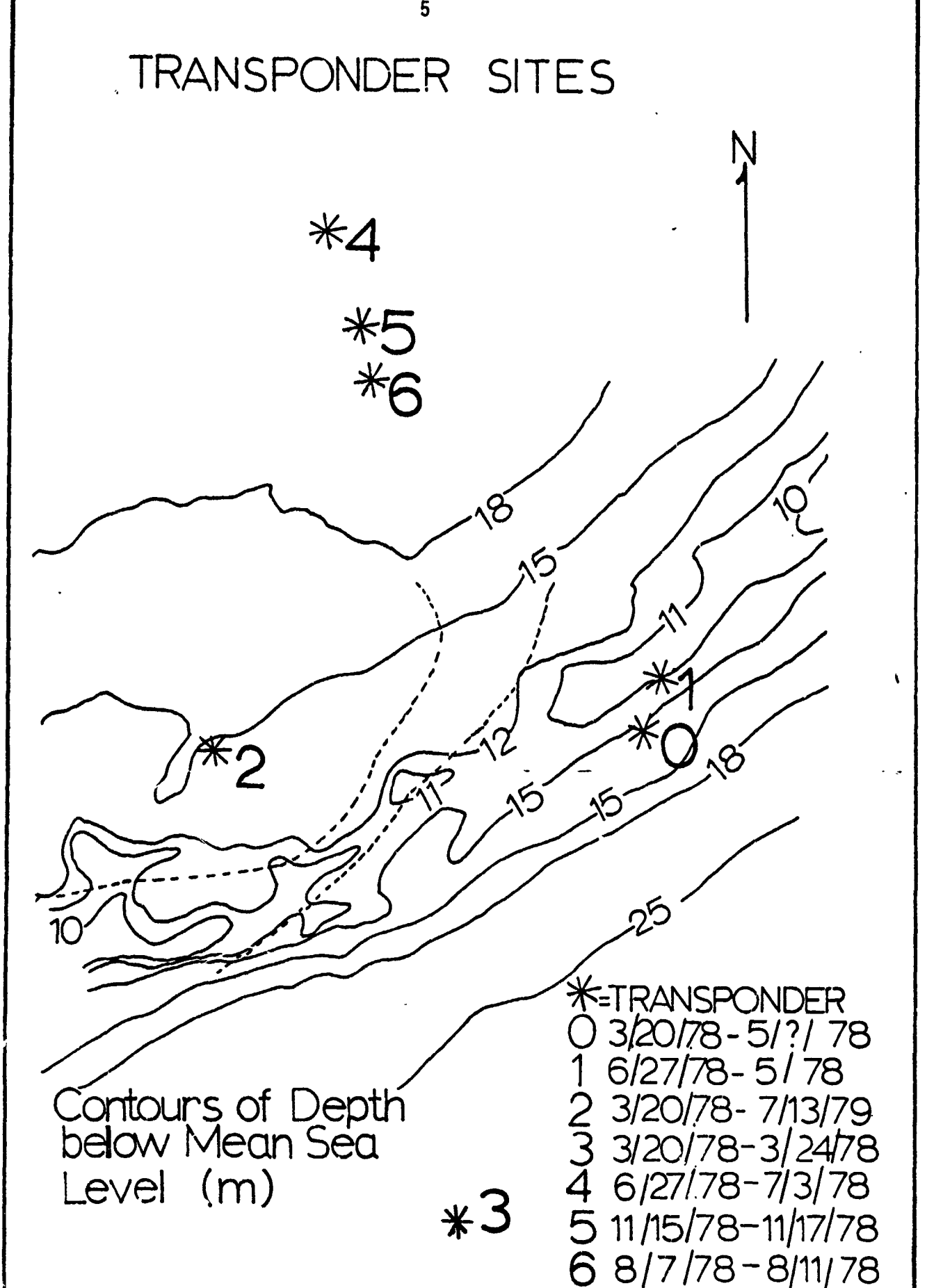

Figure 3. Locations and time periods of transponder deployment sites relative to mean depth below sea level. Dashed band outlines area of symmetric sand waves.

At first we marked the location of these transponders with surface buoys in an effort to ward off fishermen from damaging their nets and disrupting the baseline. Floats with radar reflectors were built and deployed for this purpose. Unfortunately, one of the transponder/mooring assemblies disappeared after the first transponder-navigated areal survey. It was then decided that the surface markers only attracted attention and thus were a greater threat to the maintenance of the baseline than was inadvertent dragging up of a subsurface mooring. All later work employed a subsurface mooring configuration.

To facilitate relocation of the subsurface moorings, especially during site work between surveys, when the TRANSNAV 6000 system was not aboard the vessel, small 7.5 kHz locating pingers (ORE Model 285) were attached to the transponders. After using known Loran-C coordinates to position the vessel roughly over a transponder, divers used a hand-held locating device (ORE Model 284) to swim to the transponder.

Prior to the second areal survey a new baseline transponder had to be deployed at the northeast end of the baseline in about the same location as the former, somewhat reducing our confidence in survey intercomparisons between the first survey (March 1978) and all later surveys. Fortunately calibration lines were run, during which Loran-C and TRANSNAV 6000 fixes were simultaneously recorded, in order to relate each transponder configuration to the local Loran-C coordinate system. Using the Loran-C coordinate system common to all transponder configurations, it was possible

to rotate each survey about the permanent southwest transponder location with a great degree of confidence (Fig. 4).

In all surveys during which the shipboard X-Y plotter was used to guarantee nearly complete seafloor coverage with ship tracks as nearly parallel as possible, ship's position was plotted every 2, 5, or 10 seconds, as selected. Simultaneously a keyboard print-out provided a permanent listing of fix time (hr, min, sec), ship's position in an X-Y coordinate system related to the three transponders, ship's course, and ship's speed. This keyboard information was generally requested by the operator every 50 seconds, the fix in question was noted and numbered sequentially on the X-Y plotter, and all ongoing geophysical records were time-event marked and numbered at the instant of the outgoing pulse from TRANSNAV 6000 shipboard transducer to the transponders.

The accuracy of the navigation system is estimated by the manufacturer to be $\pm$ 3 meters. An indication of the quality of this estimate is provided by comparing the three estimates of baseline length measured during calibration of the June, August, and November 1978 transponder grids. These lengths were 882.3 m, 878.8 m, and 878.9 m, respectively, or 880.0 m $\pm$ 1.5 m.

Areal Surveys

Data collection was designed to account for likely response times of the various sedimentary bed forms present. Monitoring of the sand waves required accurately navigated geophysical surveys at intervals of a few months. For this purpose, four surveys were made over a period of 238 days (Table 1). Each survey

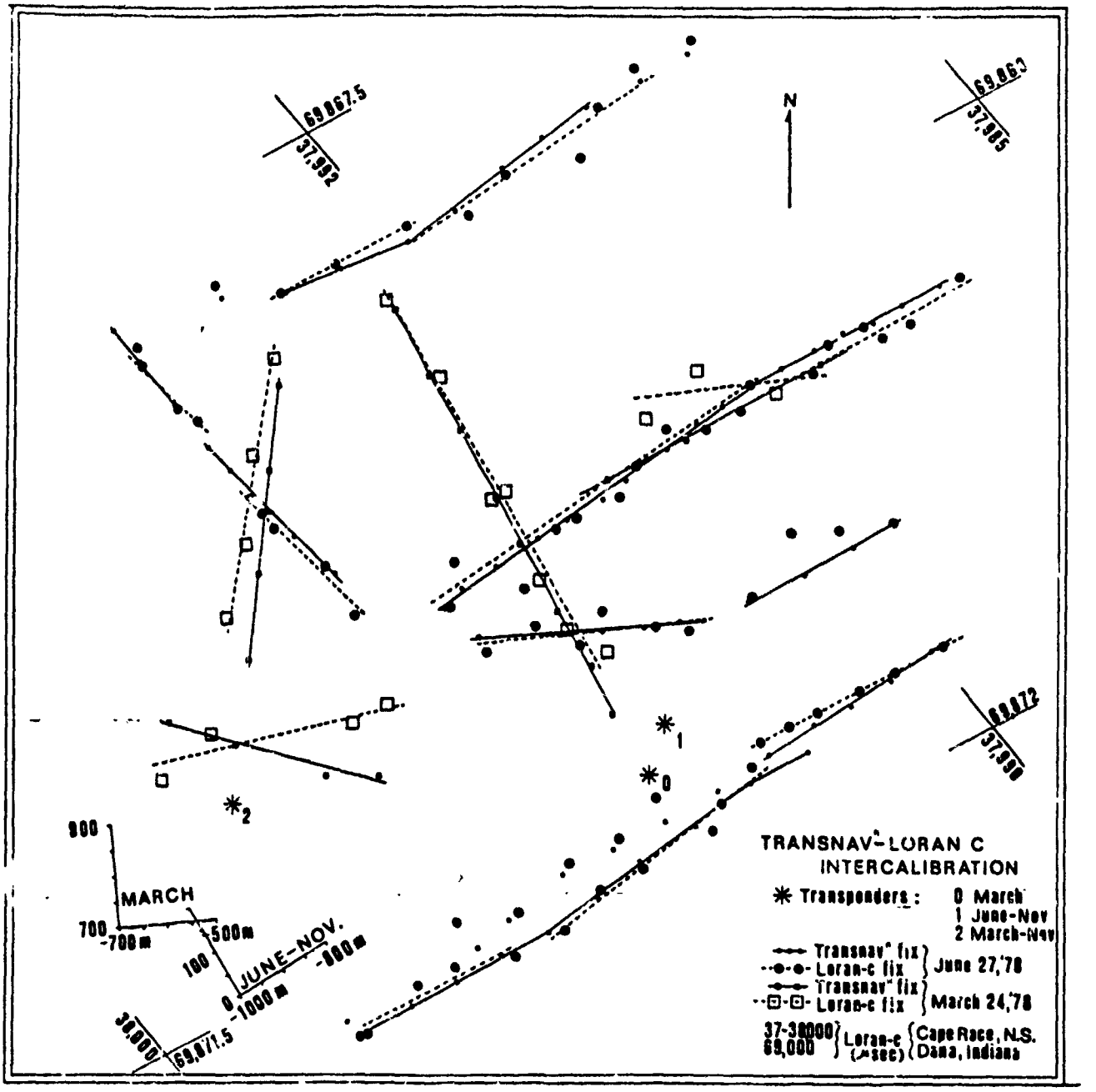

Figure 4. Relationship between the transponder coordinate systems for each areal survey and the local Loran-C navigation grid. In order to relate the March survey (transponder baseline 2-0) to all the other surveys (transponder baseline 2-1), calibration tracks were run in March and June during which ship positions were recorded relative to both Loran-C coordinates and the associated transponder array. Loran-C positions were plotted on the Loran-C grid, and least-square fits to these less precise positions drawn to best represent the true ship tracks. Transponder-navigated charts of the same ship tracks were then fit by eye to their Loran equivalents, keeping the position of transponder #2 common to both surveys. Transponder #2 was known to be "fixed" by the relation of its anchor to diver-emplaced stakes for the duration of the study. The excellent control along the NE-SW trend restricts significant alignment errors to small rotations about transponder #2 in a way that position errors for a given point between surveys would increase with distance from this point, but only in the direction of the rotation vector (approximately NW-SE) Position errors in the NW-SE direction are ergo parallel to most sand-wave crests, and are thus far less important than position errors along trends perpendicular to these crests.

TABLE 1

TRANSPONDER-NAVIGATED CRUISE SUMMARIES, 1978

Dates	Comments
March 20-24	First Areal Survey
June 27-30	Second Areal Survey
July 25-August 10	Testing of Tetrapod System
August 10-11	Third Areal Survey
Sept 5-8	SCUBA Diving Work on Superimposed Bed Form Migration
Oct 10, 27	SCUBA Diving Work on Superimposed Bed Form Migration
Nov 1-10	Tetrapod Deployments
Nov 15-17	Fourth Areal Survey

used a high-frequency, narrow-beam echo sounder (200 kHz, fish-mounted transducer, Raytheon Model 719), and sometimes a side-scan sonar system (ORE Model 170c), all time-correlated to the TRANSNAV 6000 navigation system.

Site Studies

To study the smaller bed forms superimposed on sand waves, a tetrapod was designed to support a 35 mm camera and flash, a 4 mHz echo-sounder, and an acoustic-travel-time current meter with sensors at approximately 30, 50, 100, and 300 cm from the bed (Fig. 5). The current meter, coined BASS (Benthic Acoustic Stress Sensor), was designed and built at WHOI by Williams and Tochko (Tochko, 1978).

Because of the extremely complex flow regime within the sand-wave field, a series of tetrapod deployments was made over the "first wave" on the ebb-dominated northeastern edge of the study area. This sand wave was chosen because of its position downstream (southwest) of fairly flat sea floor, since this environment was expected to be conducive to a simpler mean-velocity field. In addition, the northeastern end of the transect, upstream of the first wave, was a site used to establish the "reference" velocity field against which measurements above sand waves could be compared. But with respect to smaller bed forms, the complicated sedimentology of this area made it unrepresentative of the rest of Middle Ground Shoal. Diving observations of the first wave showed it to be somewhat atypical, with ripple presence being patchy, apparently in response to local variations in sand size.

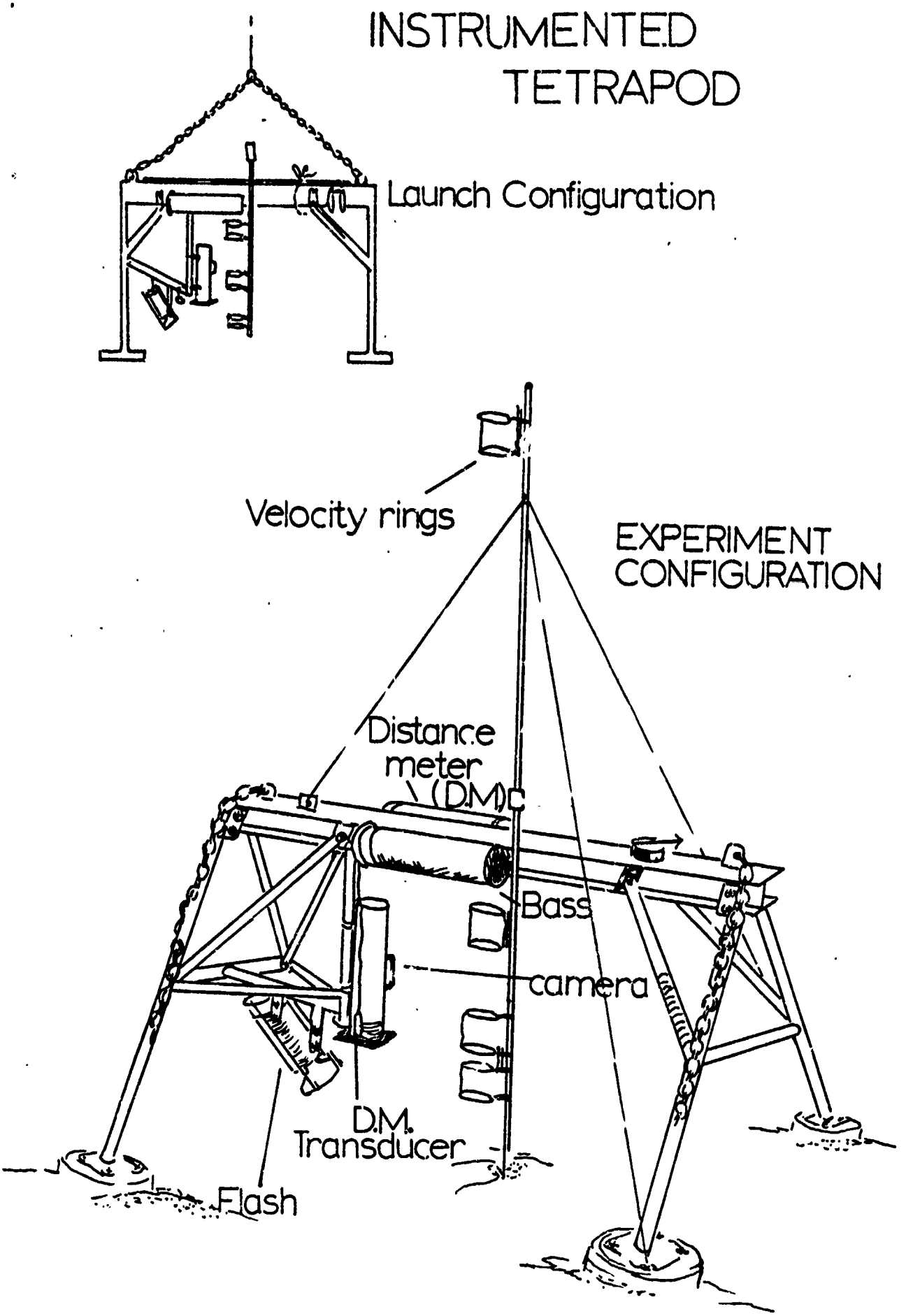

Figure 5. Launch and experiment configuration of the instrumented tetrapod. The mast to the top velocity sensor is assembled by divers on the seafloor. The lower half of the sensor mast is pushed into the bottom for stability, resulting in the 100 cm ring being lowered away from the influence of the beam.

All velocity information was collected on a self-contained Sea Data digital cassette recorder; each tape could store approximately 38,000 scans of data, corresponding to a maximum data collection period of 38,000 x 0.75 sec, or just under eight hours. In order to extend this collection period to cover a full flood-ebb tidal cycle, a burst cycle was programmed into BASS (Fig. 6). The resulting data stream, although still containing approximately eight hours of information, covered an elapsed time of just under thirteen hours. The five desired deployments were on five consecutive days from 6 November to 10 November 1978 (Fig. 7).

To monitor migration of larger bed forms superimposed on sand waves, a diving transect was established over the profiles of two sand waves. In order to maintain a staked grid over a period of weeks without any surface expression of its location, the southwest transponder anchor was chosen as the origin of this line, since the attached acoustic pinger made diver relocation easy. Although this site was chosen largely for convenience, it was representative of the megarippled sand waves on the ebb-dominated flank of the shoal. A 100 m length of 3/16" nylon line was marked in one-meter increments, fastened to the transponder anchor, and staked every five meters at a bearing of approximately 230° magnetic. Diver depth-gauge readings were taken at five-meter intervals along this transect, as well as at the crests and troughs of the larger bed forms. Divers occupied this transect on 6 September, 8 September, 13 October, and 27 October 1978 (Fig. 8; Transect C of Fig. 9).

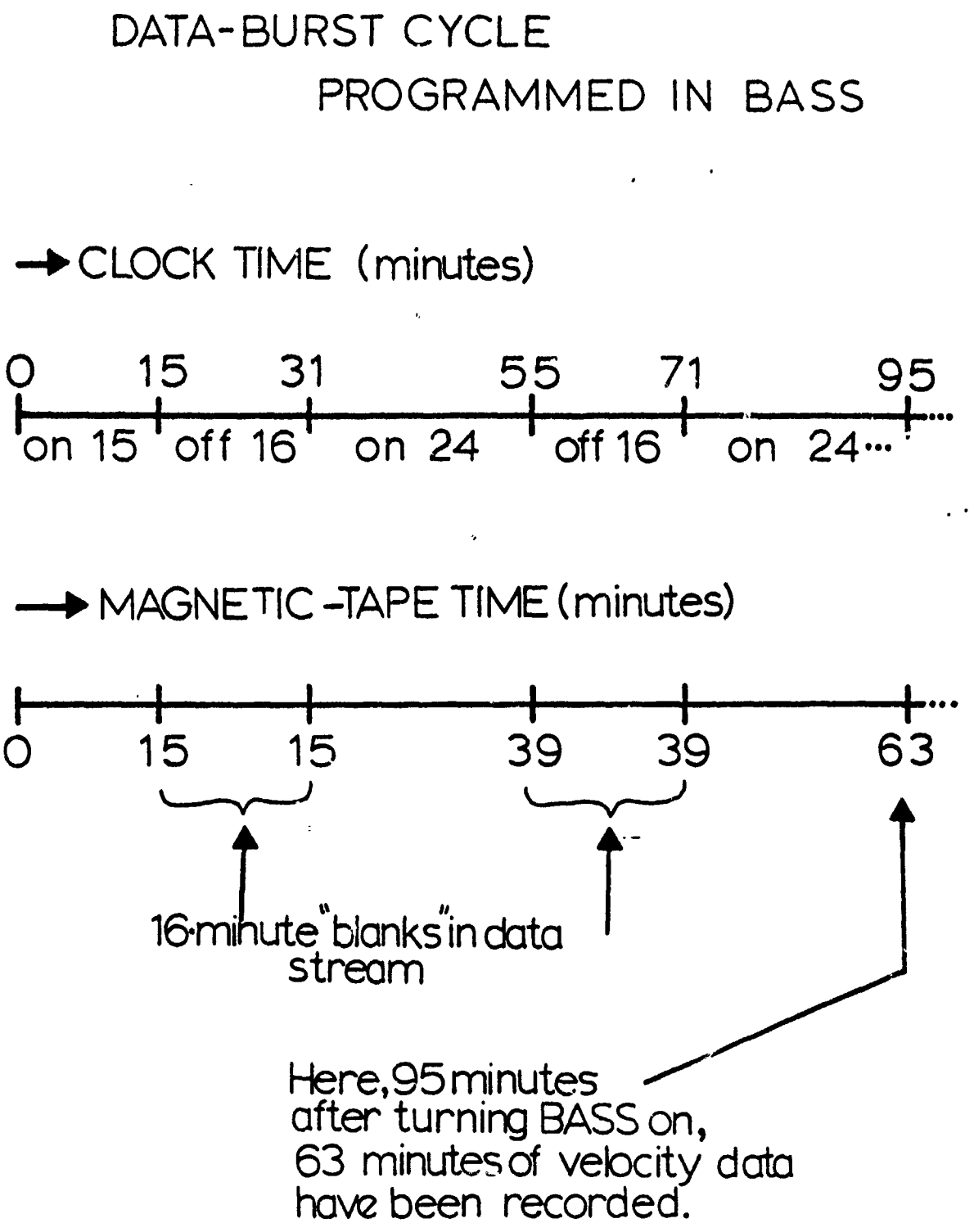

Figure 6. On/off data acquisition cycle programmed into BASS. After an initial "on" period of approximately 15 minutes (1200 data scans at a 0.75 second interval), during which the plastic bags provided zero-offset data for each sensor pod, BASS recorded data in a 16-minute off (1280 scans)/24-minute on (1920 scans) cycle. A "clear leader" of magnetic tape delayed data acquisition after BASS was turned on for 50 to 150 scans, reducing this first "on" cycle to 13.1 to 14.4 minutes. The exact scan count for this first cycle was read from analog records of the raw BASS data (made for determining zero offsets), and all velocity calculations run for time blocks exactly divisible into 24 minutes starting at the end of this first data cycle.

Figure 7. Transect of tetrapod deployments in map and profile view. The two bathymetric profiles of 11/15/78, whose track lines are shown dotted, have been projected to the solid straight lines which best represent their mean bearings, and these idealized track lines have been made 14-meter datum levels. The central profile, for which there is no track-line coverage, is an interpolated profile for this intervening position, the lack of a double crest reflecting diver observations over the crest of the trough deployment site. The trough-to-crest height drawn on this interpolated profile also reflects depth-gauge measurements made by divers during this experiment. The tetrapod deployment sites can be seen relative to the profiles, the tetrapod having been drawn to scale.

The transponder-navigated grid can be referenced to Figure 4. The tetrapod sites in map view are shown as circles relative to this grid.

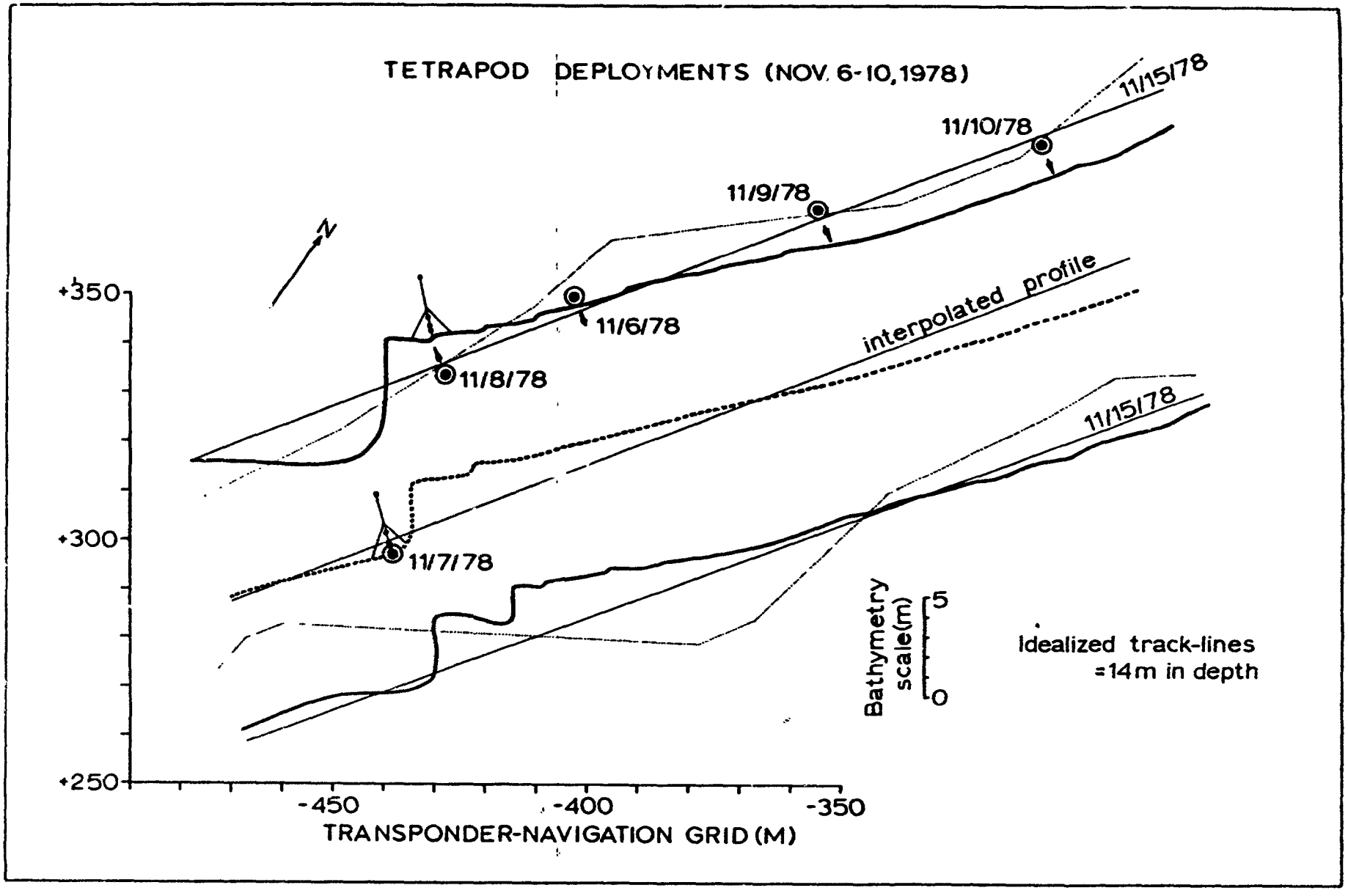
TETRAPOD DEPLOYMENTS (NOV. 6-10, 1978)
11/15/78
11/10/78
11/9/78
11/6/78
11/8/78
11/7/78
interpolated profile
11/15/78
N
+350
+300
+250
-450
-400
-350
TRANSPONDER-NAVIGATION GRID (M)
Bathymetry scale(m)
5
0
Idealized track-lines
=14m in depth

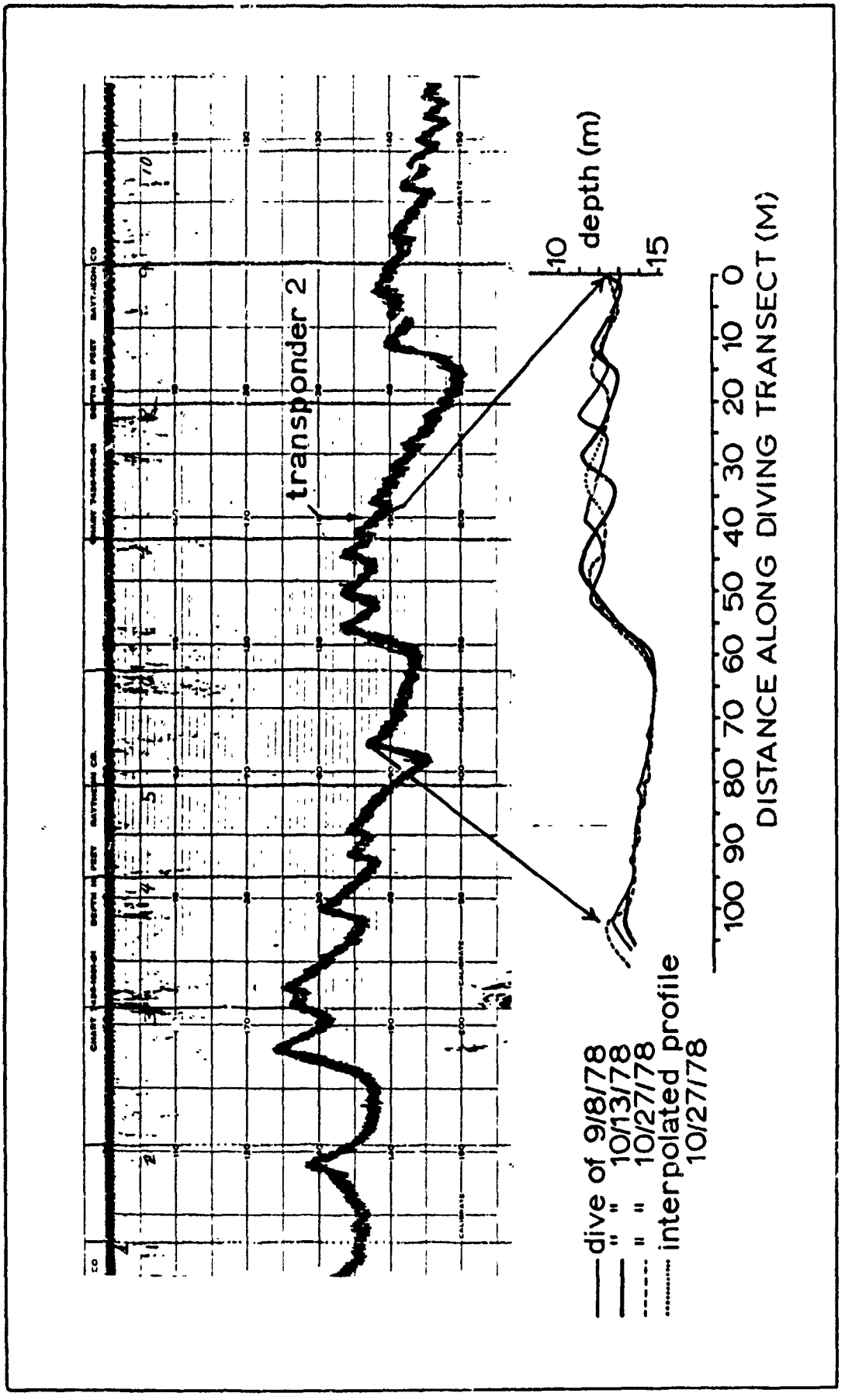

Figure 8. Summary diagram of SCUBA measurements of megaripple migration, transect C. Dotted part of 10/27/78 profile indicates part of wave where measured line was buried. Bathymetric record was taken over the diving transect on 8 September 1978.

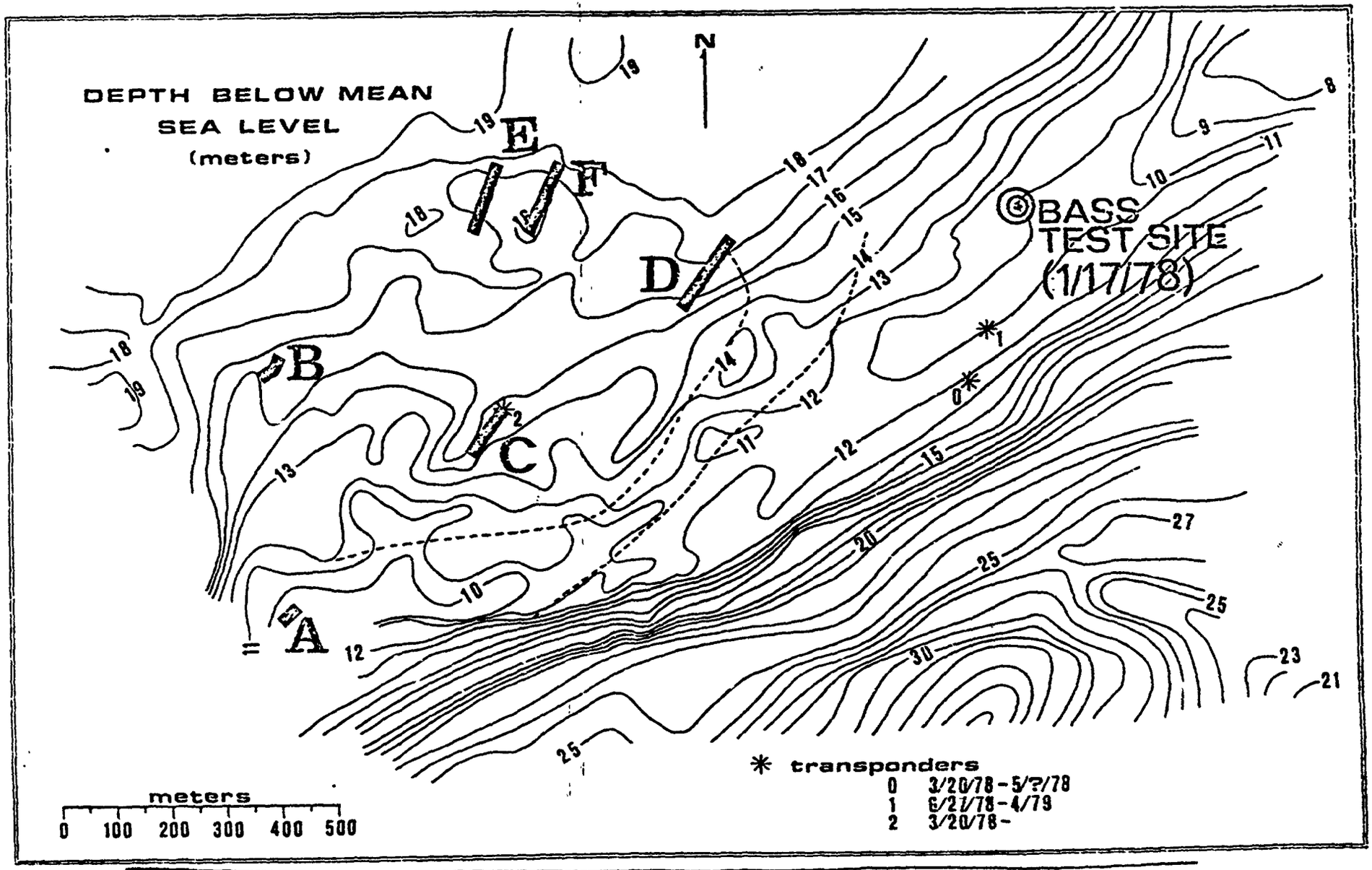

Figure 9. Chart of SW Middle Ground Shoal showing position of sediment sampling transects A-F and location of a test deployment of BASS on the flood-dominated flank of the shoal.

Since it was known that grain size varies sharply over short distances on the shoal because of the presence of the sand waves themselves, it was decided not to make an areal survey of sediment size. Instead, diver-collected bottom samples were taken at tetrapod sites, and sampling transects (45-105 m long) were carefully laid out over individual sand waves using the same techniques as for monitoring bed-form migrations (Fig. 9).

Results

Basic Features of the Shoal

Comparison of the chart of depth below mean sea level (Fig. 9) and the chart of sand-wave profiles (Fig. 10) shows that the trend of the 17 m and 18 m isobaths in the north-central portion of the study area expresses well the boundary of the sand-wave field. The "first wave," chosen for detailed flow measurements, can be seen on Transect D in Fig. 9. Sand waves on the northern flank are ebb-dominated (lee slopes facing southwest), and those on the southern flank are flood-dominated (lee slopes facing northeast), reflecting the pattern of tidal flood and ebb dominance. A band 100-200 m wide lying roughly along the crest of the shoal (dashed in Fig. 9) is best described as a zone of symmetrical sand waves.

Analysis of sand-wave height and spacing shows that the mean spacing of the asymmetrical forms (74.9 m) is approximately 1.7 times that of the symmetrical forms (45.2 m), while the mean height of the ebb-oriented waves (3.44 m) is greater than that of either the symmetrical (2.39 m) or the flood-oriented (2.46 m)

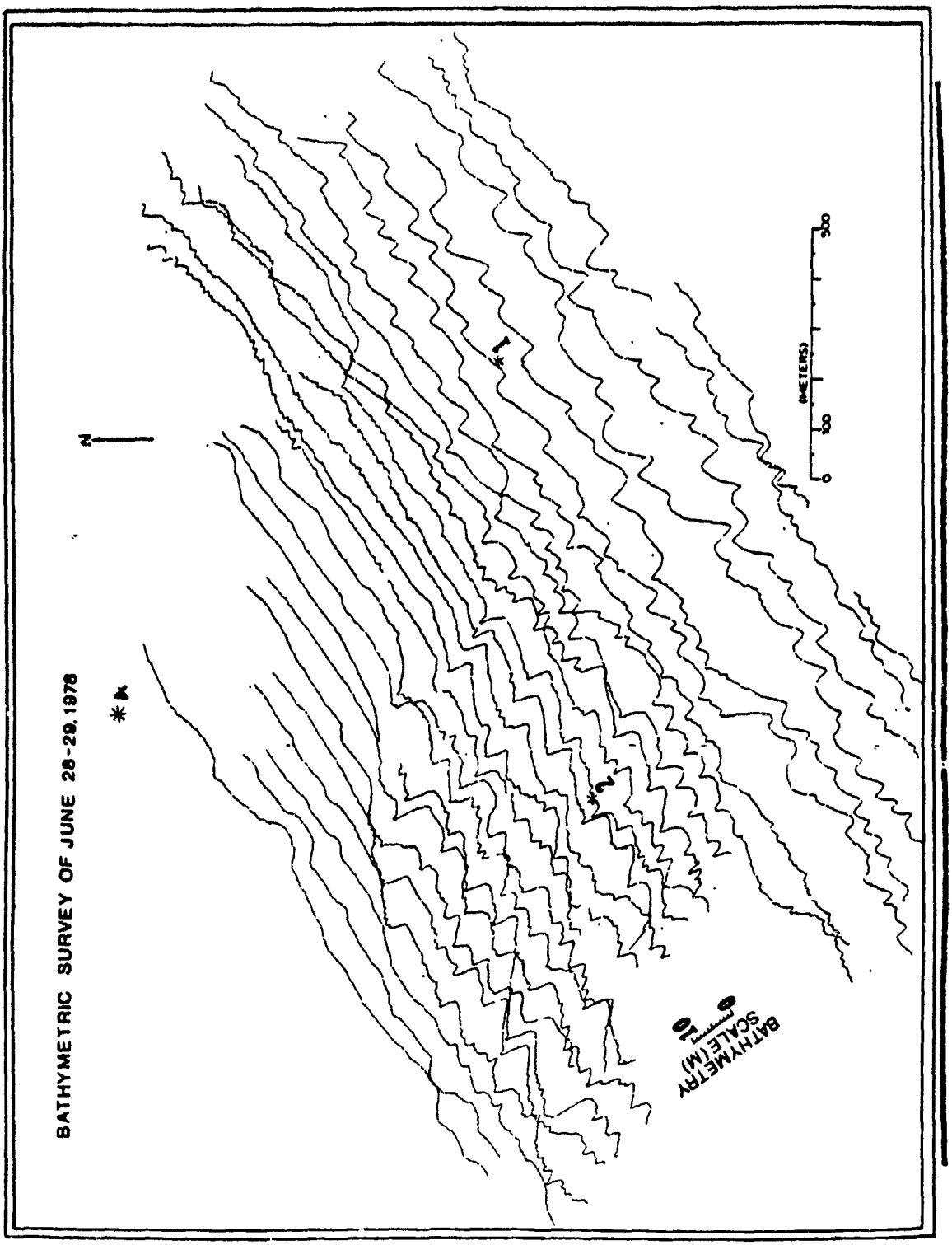

Figure 10. Chart of bathymetric profiles projected along track with track lines removed for clarity. Bathymetric scales are aligned along projection angle of original computer plot. Survey of 28-29 June 1978.

waves. There does not appear to be any correlation between local sand-wave height and water depth. Further analysis of Fig. 10 shows that the ebb-oriented waves on the northern flank tend to have stoss slopes ranging from concave to slightly convex, the larger ones often covered with smaller bed forms. The flood-dominated southern flank, however, generally exhibits sand waves with rather convex slopes, far fewer showing superimposed bed forms. Many of the ebb-oriented waves are reminiscent of the "cat-back" profiles first described by Van Veen (1935), while the flood forms are more like ripple profiles generated by unidirectional flows in flumes. Sand on the northern flank is coarser than on the southern flank (0.71 mm vs. 0.34 mm), although many more samples must be collected to characterize better the southern flank.

Observations on sediment size, combined with a simple analysis of incipient conditions for bed-load and suspended-load transport (Miller et al., 1977; Bagnold, 1966) and with an estimate of the relative importance of tidal drifts on opposite sides of the shoal, suggest that suspension transport of sediment is far more important on the southern, flood-dominated flank (Briggs, 1980).

Local Mean-Velocity Field

The results of our preliminary analysis of the mean-velocity data collected over the profile of the first wave is summarized in Figs. 11-15, in which all velocities are 8-minute averages (each 24-minute data acquisition cycle of BASS is summarized by

three 8-minute means). Fig. 11 shows the tidal curve one meter from the bed at each of the deployment sites; Fig. 12 shows these curves superimposed on a single time axis for intercomparison. The tidal curves are quite regular and sinusoidal, except for the trough experiment (7 November), which shows the effects of sheltering by the sand wave. Maximum ebb velocities exceed flood velocities, as expected for this ebb-dominated sand wave, and the duration of the ebb tide (averaging approximately 6 hr 23 min) exceeds that of the flood (5 hr 55 min). A very regular and symmetrical pattern of flows between the ebb and flood quadrants was recorded in the sand-wave trough, with an average duration of 33.5 min for each cycle. There is a regular progression in velocity maxima over the sand-wave profile (Figs. 12 and 15) which matches the trend that would be predicted for turbulent flows accelerating over a topographic high, except that flood velocities were unexpectedly strong on 9 November and ebb velocities were unexpectedly strong on 10 November. This may be explained by weather conditions, all deployments of the tetrapod having been made on calm days except on 9 November, when strong SW winds caused surface waves up to 1.5 m high. This weather event, while enhancing flood velocities and decreasing ebb velocities during the strong winds (9 November), may well have resulted in coastal setup which enhanced ebb velocities and reduced flood velocities after the winds abated (10 November).

With only minor exceptions, the tidal ellipses were measured one meter above the bed. All show a counterclockwise rotation, which matches the net counterclockwise circulation in Vineyard

Figure 11. Variations of $\overline{U}_{100}$ (eight-minute means) with time for each tetrapod experiment. Sand-wave profile shows position of experiments relative to the wave, and flow-direction key illustrates basis for plotting velocities on flood or ebb side of zero-velocity line. The 10 November experiment started in early ebb tide, while all others started before flood. The end points of the 10 November tidal curve are lettered to show how these data were time-reversed to match the other deployments (see Fig. 12).

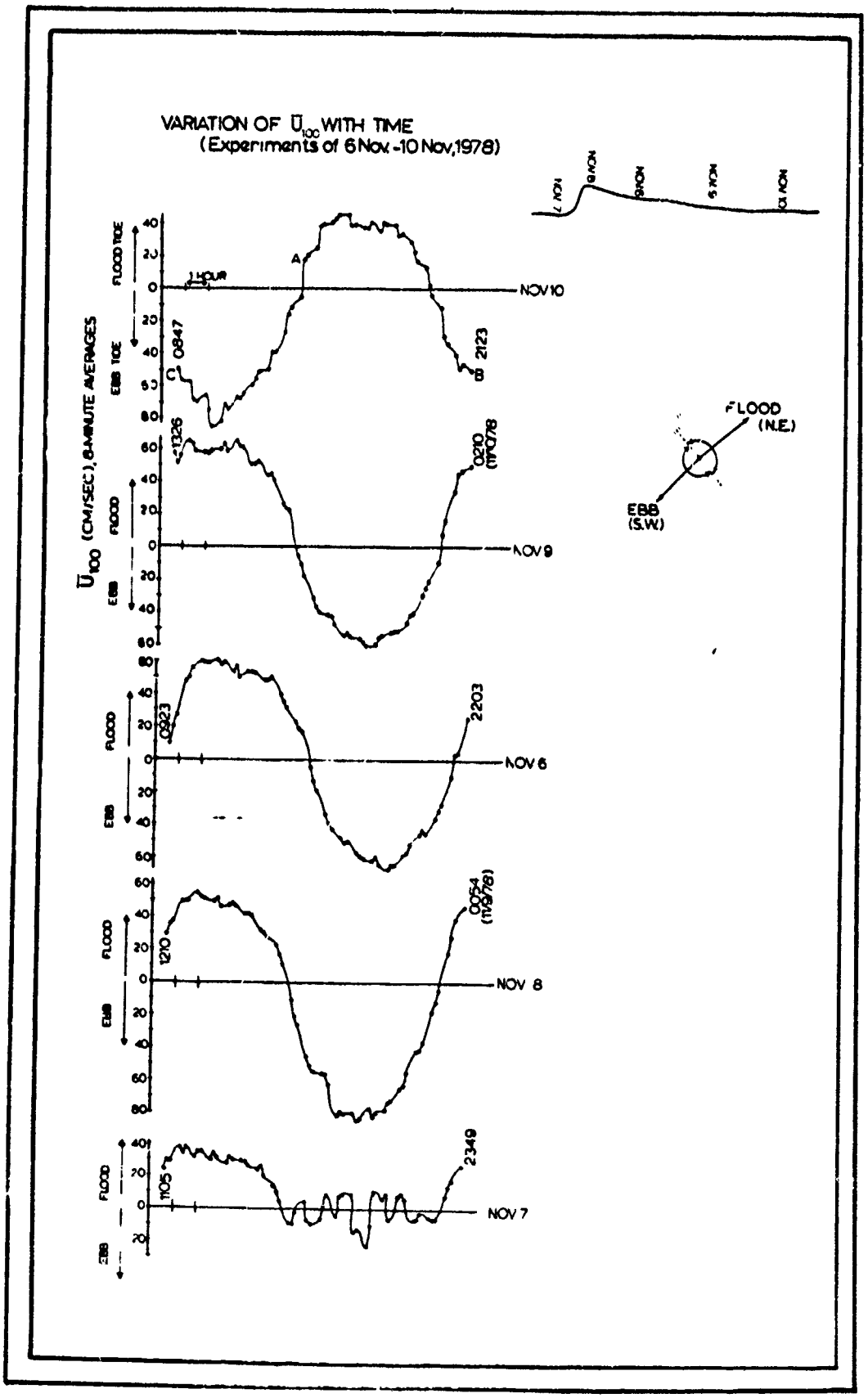
VARIATION OF $\bar{U}_{100}$ WITH TIME
(Experiments of 6 Nov.-10 Nov, 1978)
$\bar{U}_{100}$ (CM/SEC), 6-MINUTE AVERAGES
FLOOD TIDE
EBB TIDE
1 HOUR
A
B
C
0847
2123
1326
0210
(11-10-78)
0923
2203
1210
0054
(11-9-78)
1105
2349
NOV 10
NOV 9
NOV 6
NOV 8
NOV 7
FLOOD
(N.E.)
EBB
(S.W.)

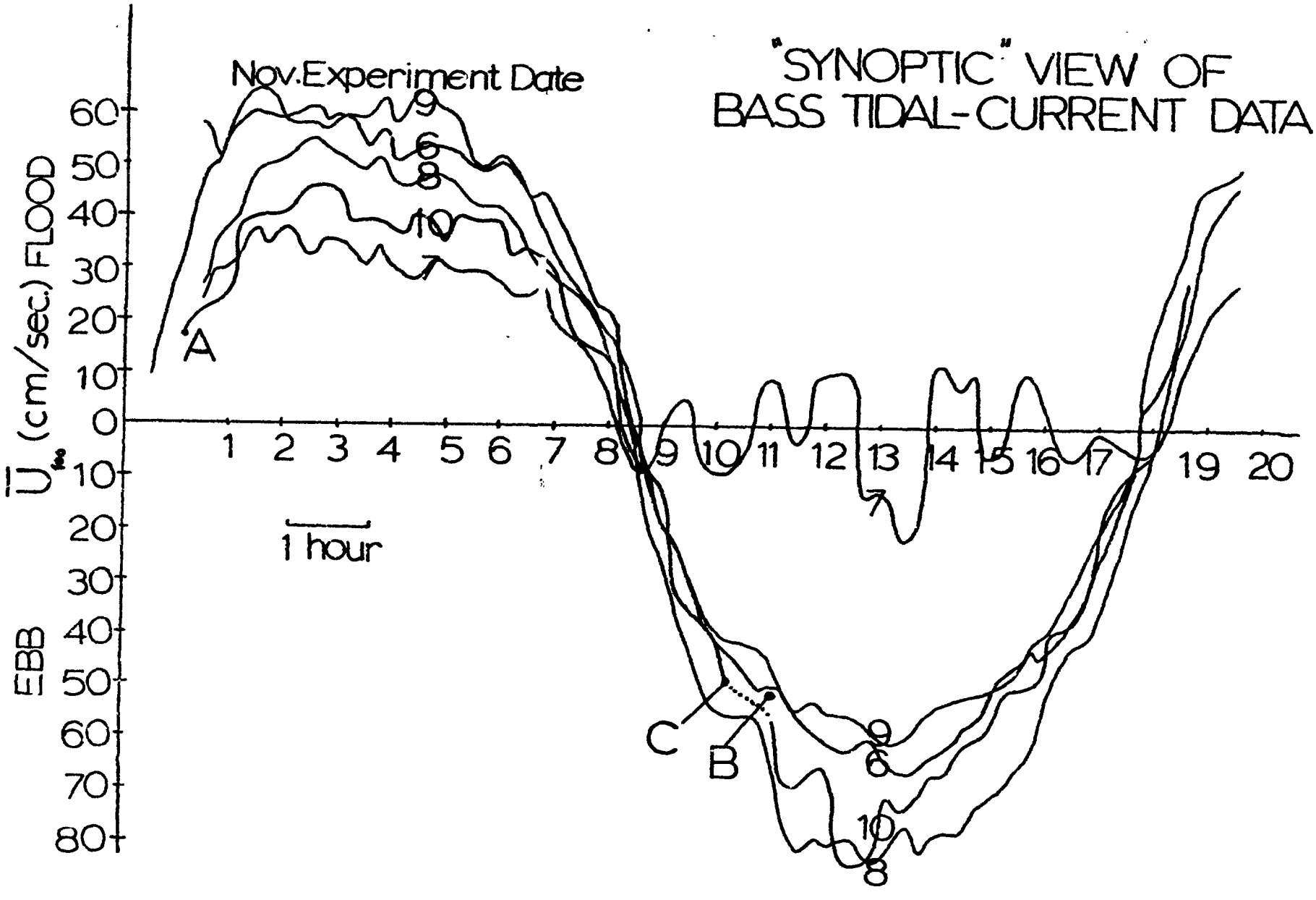

Figure 12. Tidal curves of Fig. 11 stacked on same time base for "synoptic" comparisons of velocity over the sand-wave profile. Points A, B, and C (see Fig. 11, indicate the overlap chosen to produce the most realistic ebb cycle for the 10 November experiment. Numbers 1-20 serve as "synoptic" time lines, 13 equalling the time of maximum ebb and 3 the time of maximum flood.

Sound (Fig. 13). The trough site shows ebb flows deflected significantly to the left, often at 90° or more from the direction of ebb flow over the crest. Veering of the current at each site, ranging up to 20°, is significant (Fig. 14); there is generally a counterclockwise rotation with increasing height, although the 9 November results are significantly different, probably because of surface waves. The trough site shows veering in exactly the opposite direction.

Velocity profiles at maximum ebb and maximum flood are reproduced in Fig. 15. Ebb profiles show near-bed acceleration up the stoss slope and reversed flow in the trough. As expected, logarithmic fits could be applied only during maximum ebb flows at the upstream site (10 November) and the crest site (8 November); the logarithmic layer was only 1 m thick at the latter site. Average values of z_o, found from those profiles with linear-regression correlation coefficients $\geq$ 0.9900 (Harvey and Vincent, 1977), were 0.69 cm and 3.79 cm for the 10 November and 8 November sites, respectively; these large values can be explained fairly well by estimating the thickness of the layer involved in bed-load transport (Owen, 1964; Smith and McLean, 1977a). Values of u_* for these two stations averaged 5.68 cm/sec and 9.64 cm/sec.

One of the most important aspects of these velocity measurements which may bear upon the migration patterns to be reviewed below is the cross-shoal component of flow measured in the sand-wave trough. All the characteristics of the flow field described above are consistent with a helical-flow pattern (Faller, 1963; Allen, 1970). Helical flow in sand-wave troughs may be an impor-

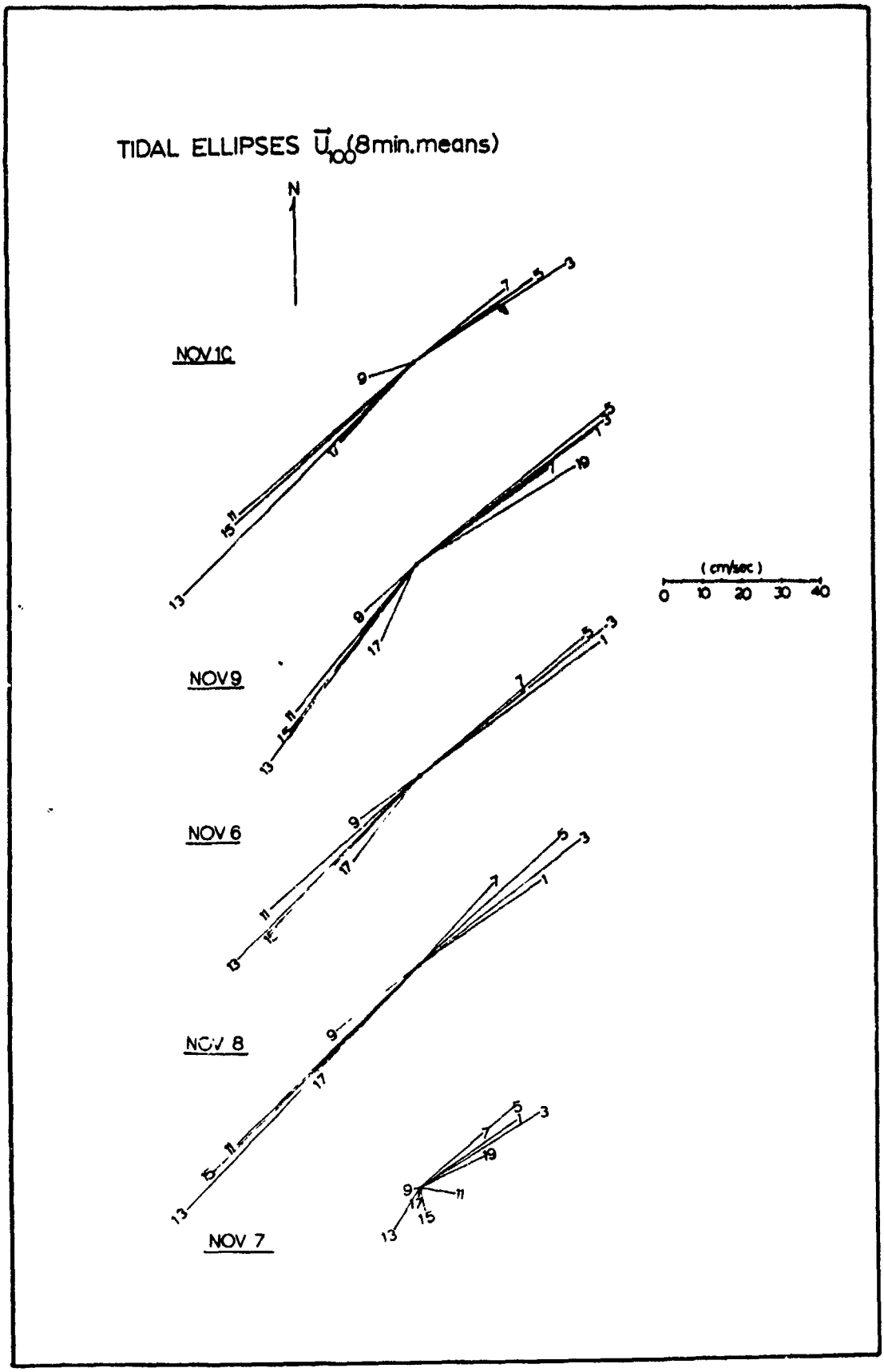

Figure 13. Tidal ellipses 100 cm above the bed, stacked in same order as previous figures. Numbers at tips of velocity vectors are time marks of Fig. 12.

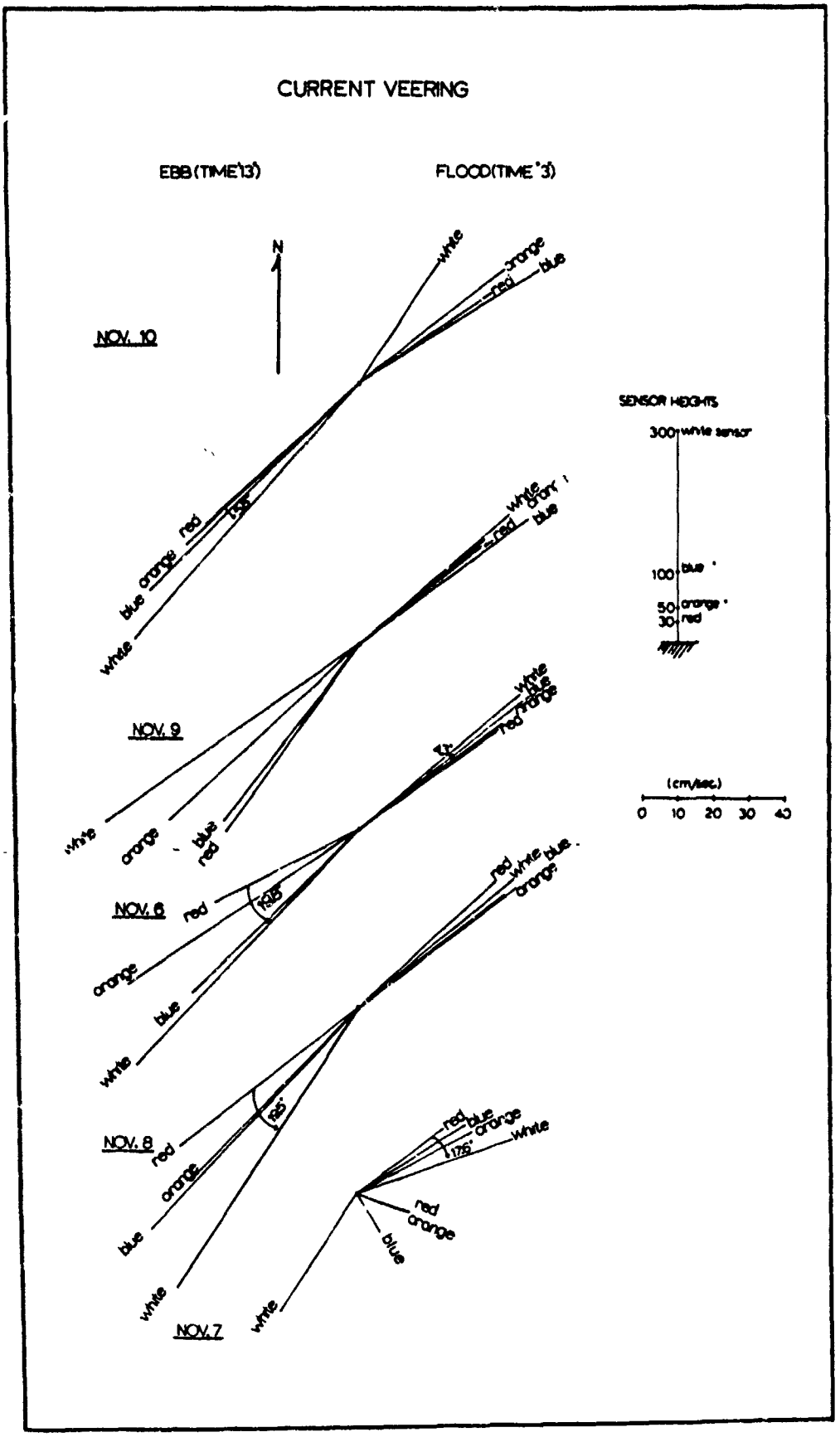

Figure 14. Mean-velocity vectors at time of maximum ebb (13) and maximum flood (3) for all four sensor heights. Colors are keyed to sensors at right of figure. Experiments stacked in same order as in Fig. 13.

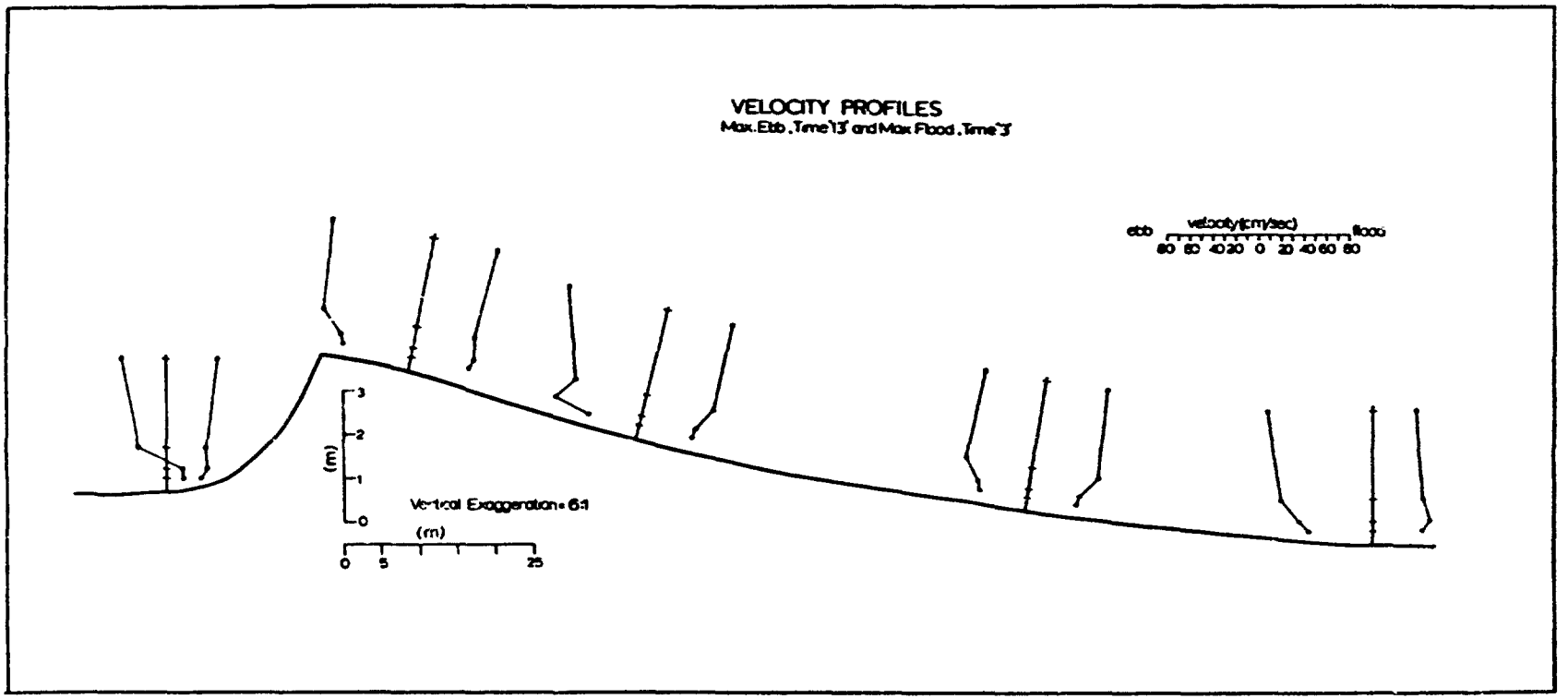

Figure 15. Schematic of velocity profiles at maximum flood and maximum ebb. Relative positions along profile were projected from Fig. 7.

tant mechanism for sediment transport parallel to sand-wave crests and at right angles to the axis of the shoal. Symmetrical sand waves might show similar helical flows that move sediment parallel to the crests; troughs of these sand waves would then serve as conduits for transport of sand from one flank of the shoal to the other even though the waves involve zero net transport of sediment normal to crests, as shown by the absence of net migration. In this regard, Bokuniewicz et al. (1977) observed that the average flow in an area of symmetrical sand waves is parallel to the wave crests. Further, if these helical flows can indeed transport significant quantities of sediment, they might help explain the sand-wave "flexing" documented in detail by us (see below) and reported by other workers (Terwindt, 1971; Langhorne, 1973) since the associated cells of net sediment drift along sand-wave crests could result in local sites of erosion and accretion.

Helical secondary flows probably explain the bed forms oriented parallel to the main flow that are often seen in the troughs of large transverse bed forms (Hunt et al., 1977). Examples of these bed forms can be seen in Fig. 16 in a section of a side-scan record collected over the first sand wave but north of the tetrapod transect.

Sand-wave Crest Patterns

Charts of crest position were produced by combining side-scan charts with the bathymetric track-line data on crest positions (Fig. 17). These charts show not only that sand-wave crests are rather similar in bearing across the shoal, but that in some cases a given crest can be followed from one flank of the shoal

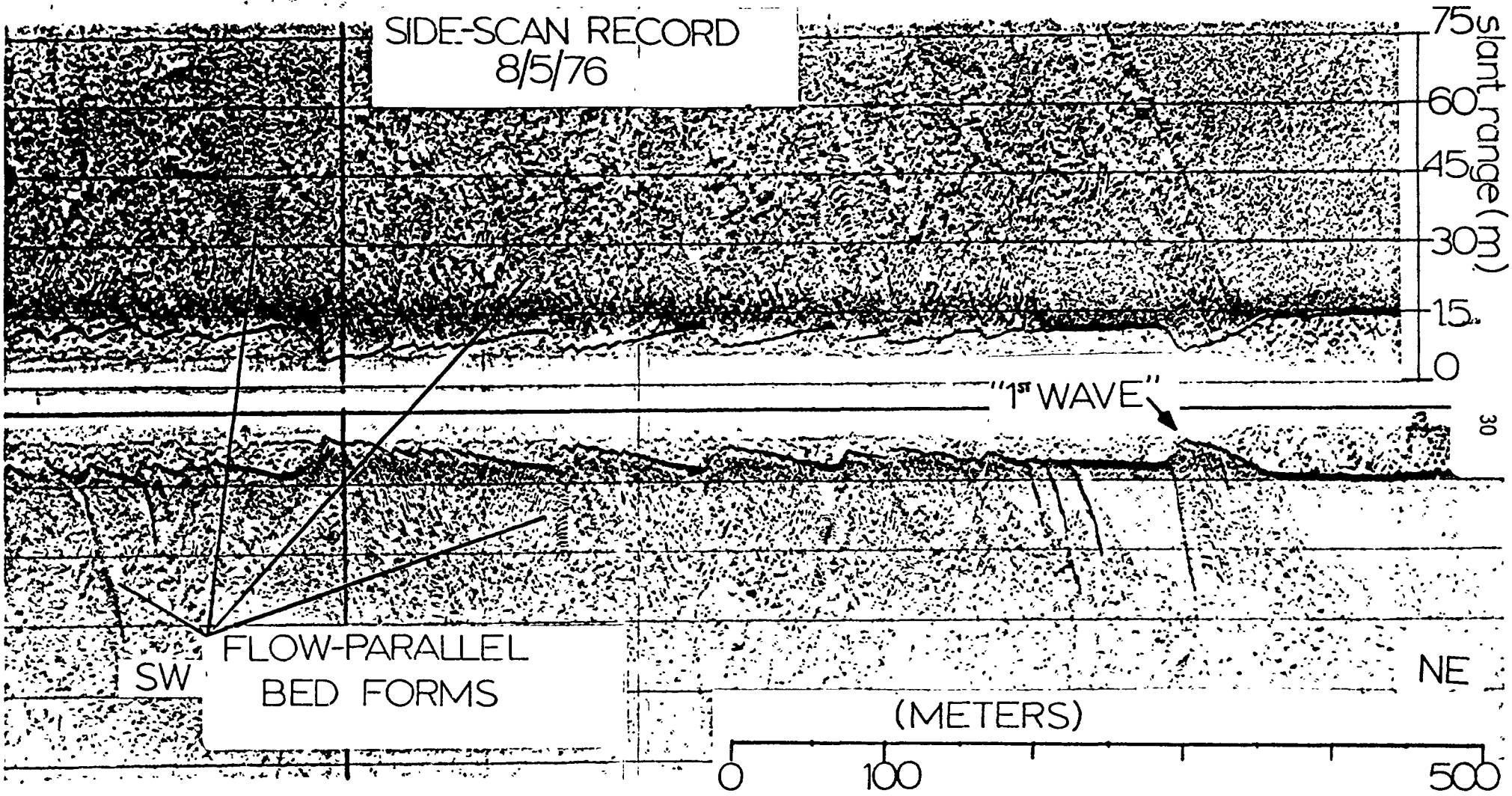

Figure 16. Side-scan sonar record (line #1, Fig. 22) showing "first" wave and presence of flow-parallel bed forms in some sand-wave troughs. "First" wave is northeasternmost symbol of line #1, Fig. 22.

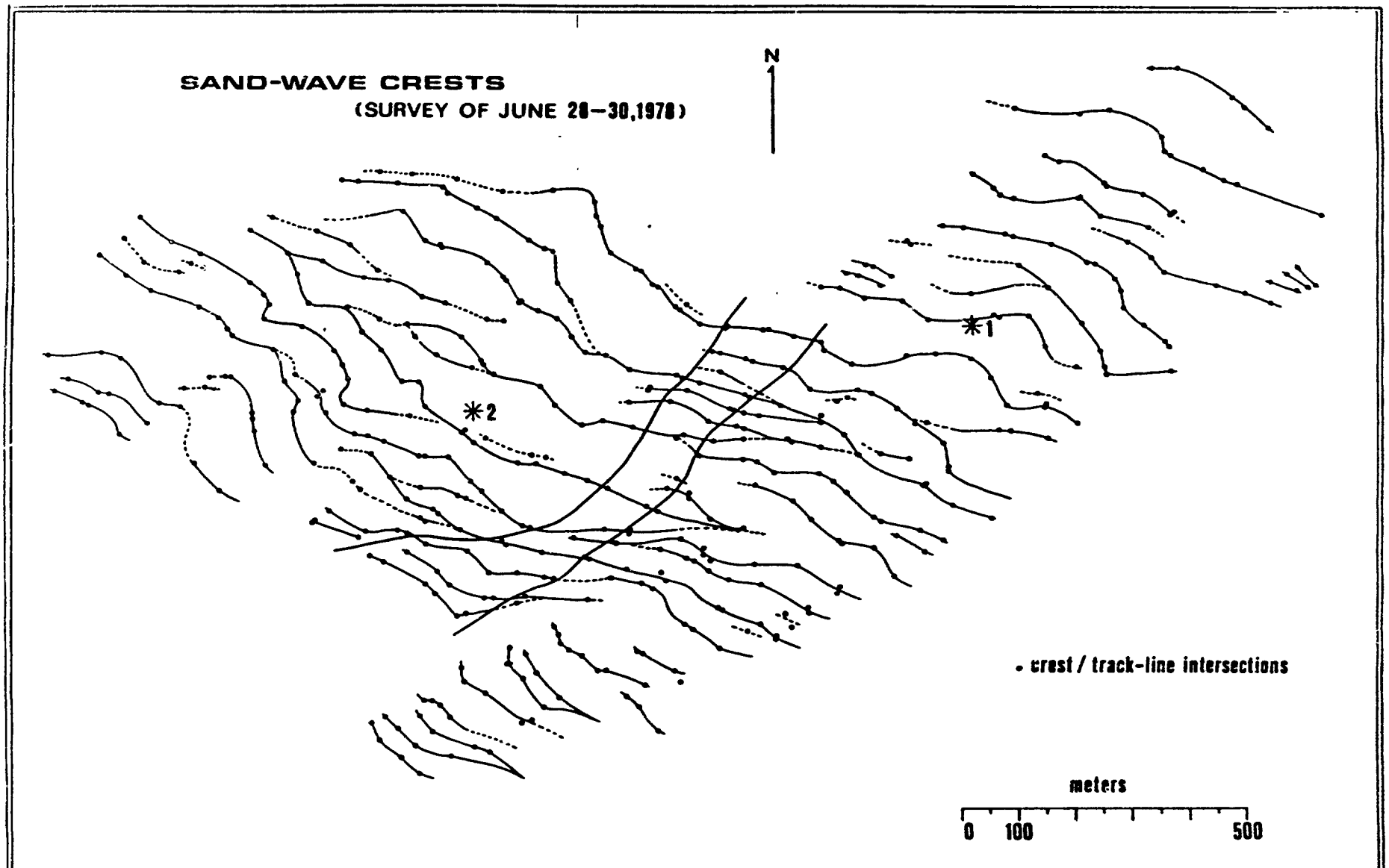

Figure 17. Sand-wave crest positions determined from the June 1978 areal survey, showing the data control of crest/track-line intersections with actual tracklines omitted for clarity. Dashed parts of the lines represent either tentative correlations or the crests of bed forms too small to be called sand waves (less than "2 by 15" meters). The 50-100 m wide band which runs roughly NE-SW midway between transponders #0-1 and #2 delineate the area of symmetrical sand waves.

to the other. These crests are oblique to the shoal axis by as much as 30 degrees (Fig. 17). Close examination of the crest-position charts suggests that the bearing of these crests changes from approximately N63°W on the southern flank of the shoal to approximately N51°W on the northern flank.

Survey intercomparisons show several important features (Fig. 18). First, as suggested by other workers (Langhorne, 1973; Pasenau and Ulrich, 1974; Bokuniewicz et al., 1977), sand waves show "flexing" of crests: migration is variable rather than uniform along crests, and in some cases even involves alternation of segments showing net forward and net backward displacement. Despite this flexing, sand waves on the northern ebb-dominated flank tend to show net displacements to the southwest and those on the flood-dominated southern flank tend to show net displacements to the northeast. Even in the belt of the symmetrical sand waves there has been some local sand-wave movement between surveys, in some places to the northeast and in some places to the southwest.

The cause of sand-wave flexing is not yet known. Better understanding of flexing may come from the observed patterns of ebb and flood cells of net migration. On the northern flank of the shoal, for which there is a reasonable data base on sand-wave migration patterns, there appears to be some degree of coherence or continuity between areas of positive (southwestward) and negative (northeastward) displacement along adjacent sand waves. This in-phase flexing may indicate the presence of small ebb parabolas within the large ebb parabola which dominates the

Figure 18. Intercomparison of crest-position charts for the March-November areal surveys. The 50-100 m wide band which runs roughly NE-SW midway between transponders delineates the area of symmetrical sand waves. The earlier crest positons were drawn without the dots which represent their crest/track-line intersections, while the more recent crest positions include these points to make possible their differentiation. Displacements were then shaded to show net ebb (to SW) and flood (to NE) displacements. Dashed lines delineate either crest lines of bed forms smaller than sand waves which still could be correlated from track to track (these features often being superimposed upon the larger sand waves), or, where data were minimal, simply tentative correlations.

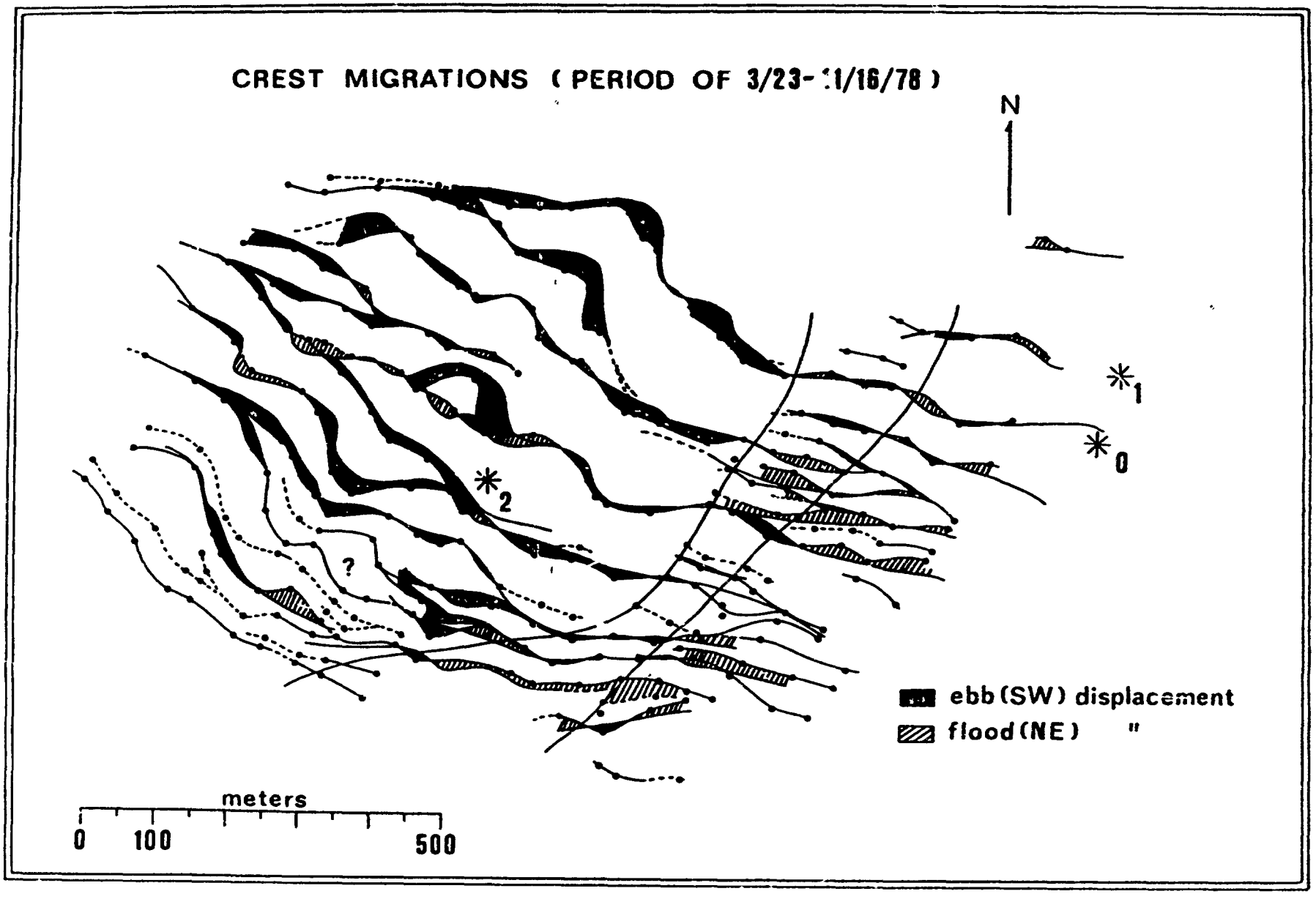
CREST MIGRATIONS (PERIOD OF 3/23-11/16/78)
N
1
0
2
?
ebb (SW) displacement
flood (NE) "
meters
0
100
500

sand-wave morphology of this flank of the shoal (Fig. 19). This concept is a small-scale analog to that of tidal parabolas described by Van Veen (1935). The migration patterns on Middle Ground Shoal suggest that these large-scale tidal parabolas may be very complex: each may contain localized "channels" with net sediment drift opposite to that of the larger parabola in which they lie. These localized channels or net-drift parabolas, whose width and length scales are similar to sand waves, are transient in their location and even in their existence, probably owing to complicated effects of topography on the tidal flow or to unknown effects of storms. More detailed study of local transport directions, perhaps by detailed mapping of the asymmetry of smaller bed forms superimposed on the sand waves, is needed to evaluate the importance of small ebb and flood parabolas.

Another point, discussed most easily with reference to Fig. 17, has important implications for the zone of symmetrical sand waves. Consider a sand-wave crest that is continuous across the shoal from flood-dominated flank to ebb-dominated flank. Our results show that, on the average, one end of this crest migrates in a direction opposite to that of the other end, with the intermediate zone (where the waves are symmetrical) serving as an approximately fixed point or pivot. If left to continue indefinitely, this pattern of migration would result in bending of the sand wave about this pivot until the overall trend is much more nearly parallel to the crest of the shoal. Sand waves would then migrate nearly straight up the flanks of the shoal.

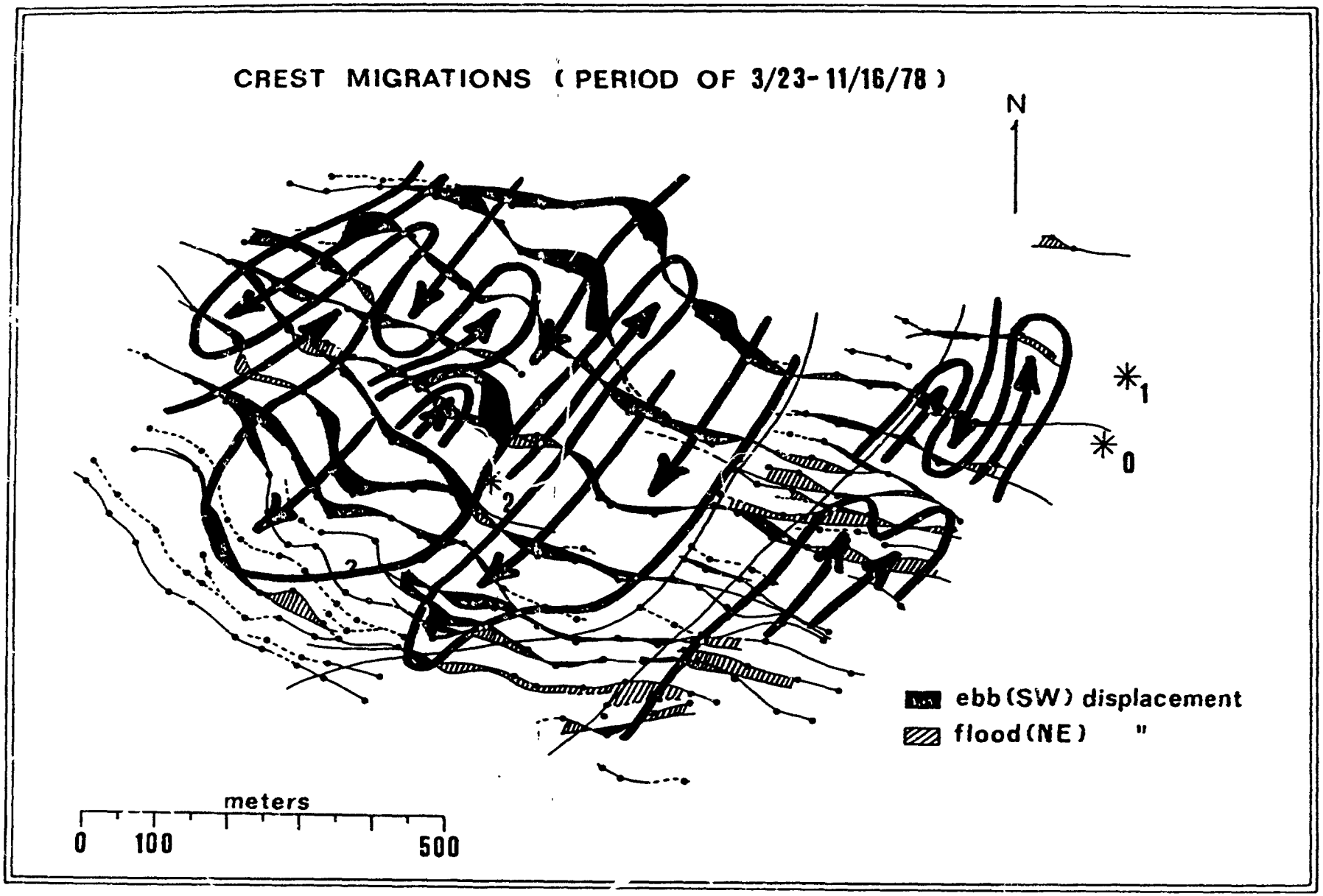

Figure 19. An interpretation of the 23 March-16 November migration period which shows the correlation between areas of net ebb and net flood migration.

Because our survey intercomparisons show that the trend of sand waves across the shoal remains fairly constant as the waves migrate in opposite directions on the opposite flanks, the continuous crests must ultimately break within the symmetrical zone by joining or branching with waves on either side.

Although considered only qualitatively here, the resulting picture of the symmetrical zone as an area of sand-wave intersection and overlap may help explain why symmetrical sand waves show smaller average spacing than asymmetrical sand waves. If two parallel sets of sand waves, one with uniform spacing of 80 m (approximately the mean spacing of the ebb-dominated sand waves on Middle Ground Shoal) and the other with uniform spacing of 70 m (tne mean of the flood-dominated waves), are superimposed within a band of overlap, the average spacing of waves within the overlap region is about 45 m, if spacings less than about 15 m are excluded (Fig. 20). Although it might seem artificial to ignore these smaller spacings simply because bed forms with such spacings have been defined as megaripples rather than sand waves, observations suggest that when two sand waves are nearly collinear one tends to become a magaripple superimposed upon the other. Furthermore, if these two wave sets merge at some small angle, as is the case on Middle Ground Shoal, the possibilities for branching, coalescence, and superposition are made all the more likely by the increased occurrence of intersections.

Comparing this mean "symmetrical" bed-form spacing of about 45 m with the average of the flood and ebb bed-form spacings, we find that the mean spacing of these asymmetrical forms is

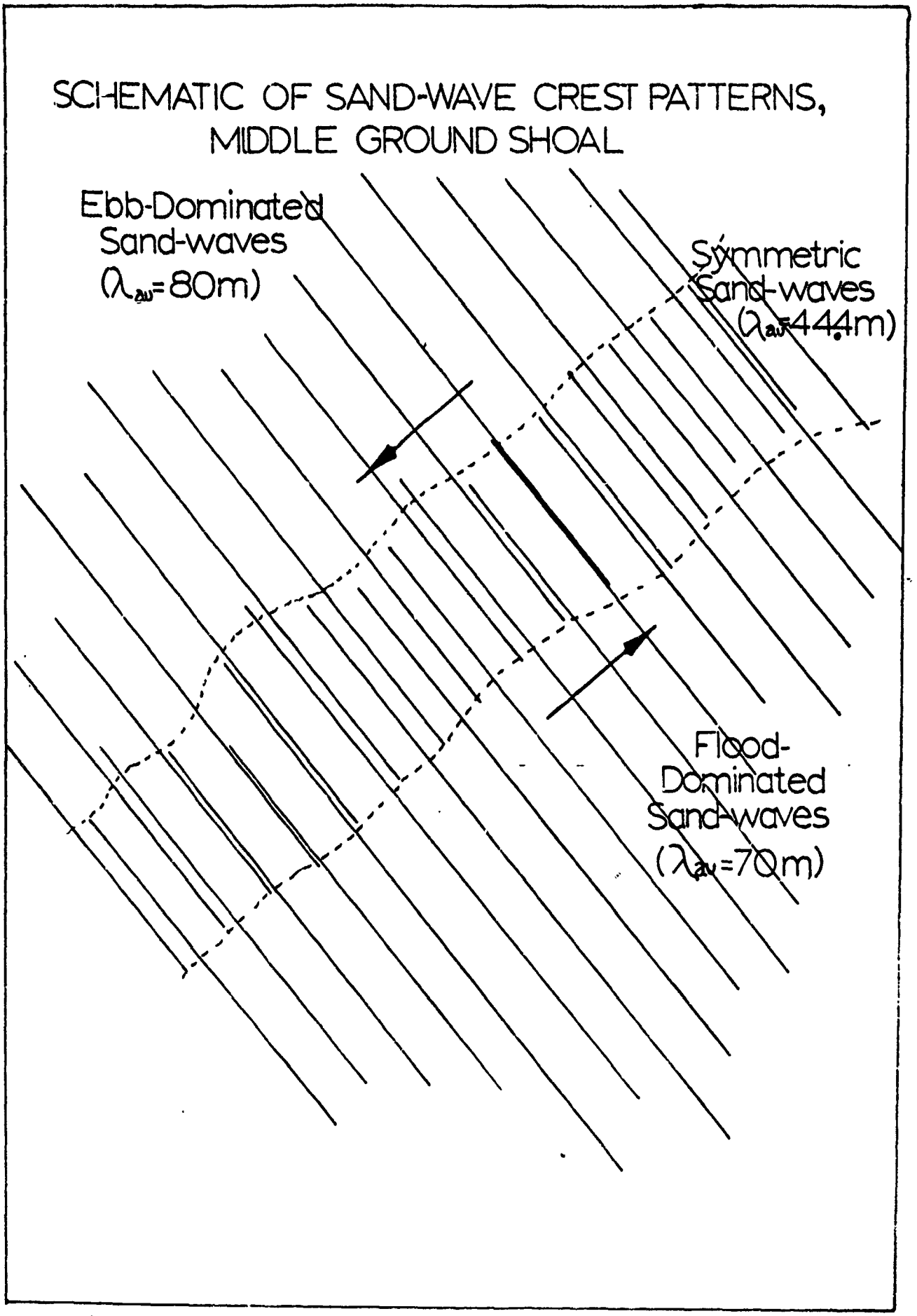

Figure 20. Cartoon to illustrate the concept of intersecting and overlapping sand-wave trains in the area characterized by symmetrical sand

approximately 1.7 times that of the symmetrical forms. Although the symmetrical part of the shoal lies along the complicated boundary between the ebb-current and flood-current parabolas, and is thus in an unusual dynamic setting, this analysis shows that the spacing of these bed forms may reflect a fairly simple intersection of two effectively independent sand-wave trains. Further study of this "zone of intersection" is needed.

Sand-wave branchings seem to be closely related to the large bed forms superimposed on the sand waves. As two sand waves coalesce, the crest of the trailing wave seems to become a superimposed bed form on the back of the leading wave, unlike the "tuning-fork" junctions seen in some other kinds of bed forms (Hollister et al., 1974) in which each crest is equally identifiable until they join to form a single crest. These observations raise the difficult question of when the subsidiary sand-wave crest ceases to be a small sand wave and becomes instead a megaripple. In view of the present confusion in classification of large-scale bed forms, we are not yet certain that this question is even a meaningful one.

Sand-wave Migration Rates

Point measurements of sand-wave migration range from -36 m to +48 m from 23 March to 30 June 1978. (Positive values indicate southwestward migration on the ebb flank and northeastward migration on the flood flank.) When extrapolated, these measurements give migration rates of -133 m/yr to +177 m/yr, respectively. Looking instead at the longest record of sand-wave migrations,

from 23 March to 16 November 1978, these point measurements are -26 m to +43 m, equivalent to yearly rates of -40 m/yr and +66 m/yr. These measurements are only an approximate indication of the maximum range of migrations that might be measured on Middle Ground Shoal, and they are somewhat difficult to interpret because they were measured without regard to local sand-wave height. Also, in view of the problems inherent in extrapolating these short-period observations to much longer periods, it would be highly desirable to obtain longer records of sand-wave migration. Fig. 21 shows sand-wave migrations averaged along the crest of each wave; the number in parentheses for each wave is the average migration rate linearly extrapolated to one year of observation.

Average yearly migration rates range from nearly zero to about 40 m/yr. As a partial test of these values, bathymetric and side-scan sonar records collected prior to this study (on 6 April 1976, 5 August 1976, and 9 June 1977) were plotted at the scale of the transponder-navigated surveys along with the crest positions as of November 1978 (Fig. 22). Since these earlier cruises were navigated by Loran-C only, much greater error bars determined from the intercomparison of Loran-C and transponder coordinates shown in Fig. 4 have been indicated for these wave-crest positions. The basic appearance of the northeastern boundary of the sand-wave field has remained very similar. Although crest positons are more difficult to identify over these longer time intervals, the position and character of the first wave makes it uniquely suited to a test of the migration rates found in this study. Assuming that the crest of the

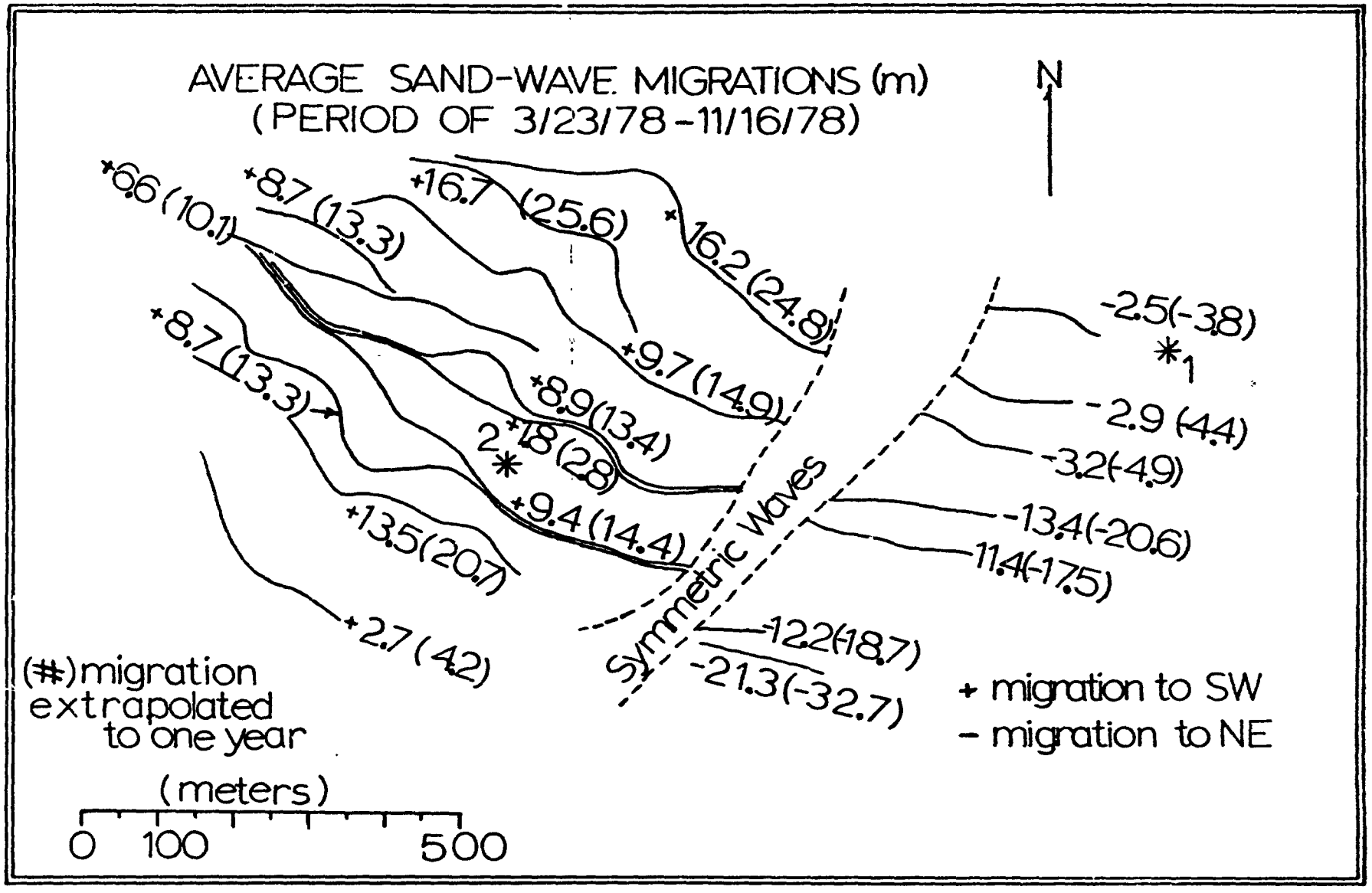

Figure 21. Chart of sand-wave crests showing average migration from 23 March to 16 November, with migration values extrapolated to one year, in parentheses. Average migrations were calculated over the crest lengths indicated by the length of each line.

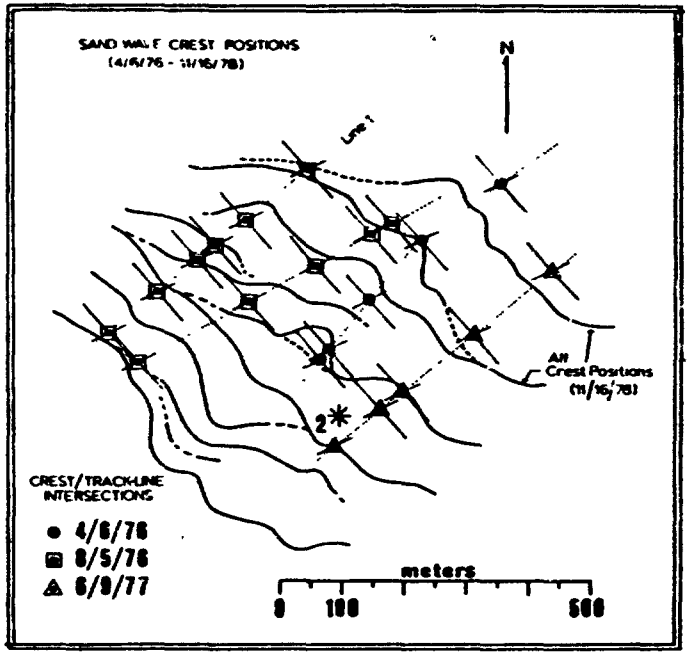

Figure 22. Chart showing sand-wave crests (as of November 1978) for north-central portion of study area with Loran-C navigated tracklines from 1976-1977 superimposed. Dated symbols indicate positions of sand-wave crests on corresponding days. Northernmost track (line #1) is shown in Fig. 16.

first wave has always migrated southwest at approximately 25 m/yr, its position on 6 April 1976, 5 August 1976, and 9 June 1977 should have been upstream of the 16 November location by 65 m, 57 m, and 36 m, respectively. The actual locations are 62 m $\pm$ 30 m for the 6 April 1976 data and 40 m $\pm$ 30 m for the 9 June 1977 data (Fig. 22). The 5 August 1976 tracks seem to show no net movement, or even negative movement, although the more southerly of the two 5 August tracks can be shifted north within its positional error bars in such a way that it too shows little net movement. All of these values are reasonably consistent with the later measurements of migration rate. The April 1976 and June 1977 results match the predicted locations extremely well, while the August 1976 results show (as this study would predict) that point measurements may indicate movements in either direction, if at all.

Sediment Transport Rates

Fig. 23 presents sand-wave migration data as a function of sand-wave height, based on migration values from the period March-November 1978. Superimposed upon this plot are curves of constant transport rate q_s per unit width of flow; $q_s = \frac{MH}{2t}$, where M is migration distance, H is sand-wave height, and t is period of observation (Simons et al., 1965). Note that there is a wide range of actual migration distances for each sand-wave height, although the spread diminishes as sand-wave heights increase. This shows that the actual point measurements of net migration on Middle Ground Shoal do not bear a simple relation

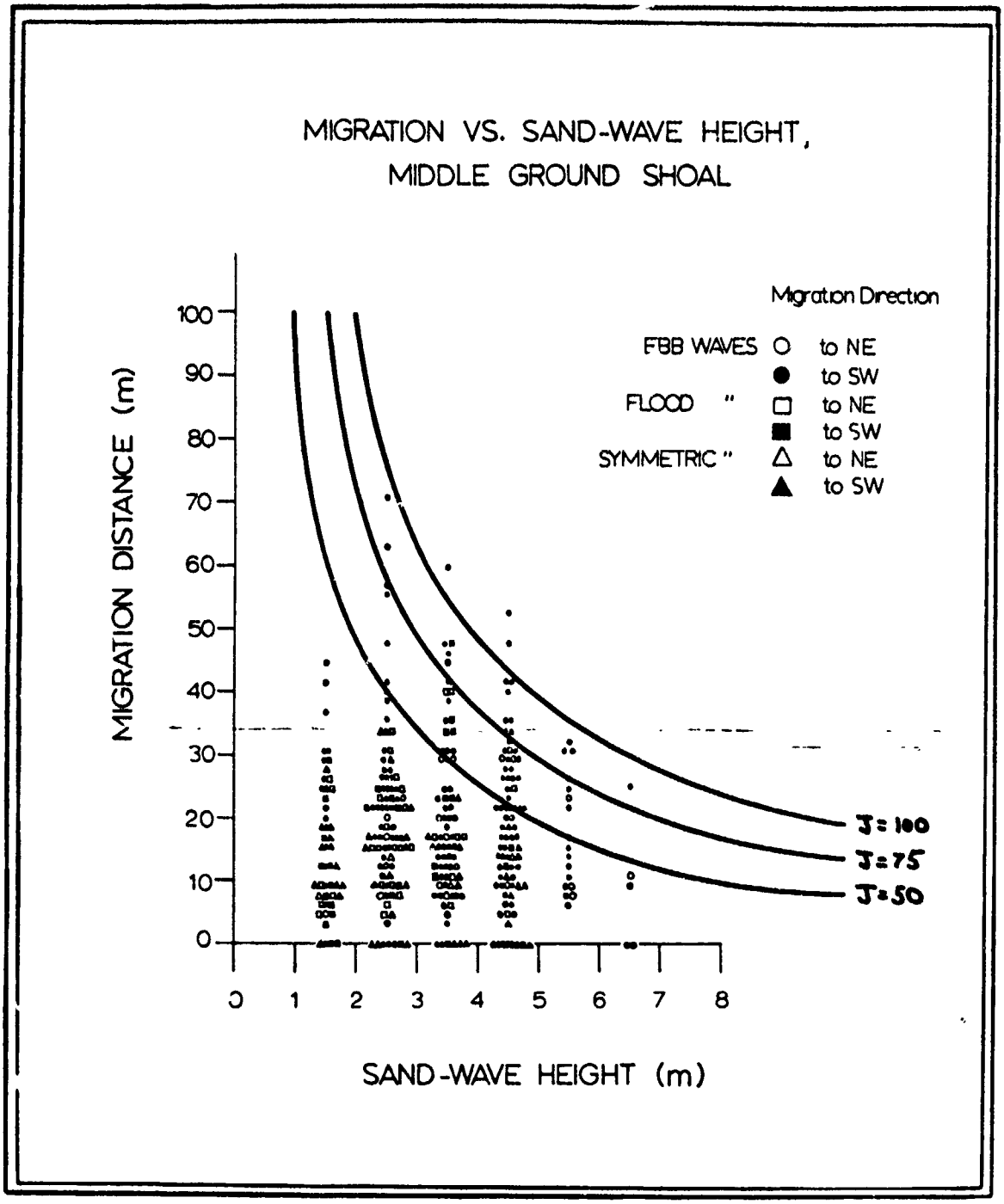

Figure 23. Relation between sand-wave height and net migration (period of 23 March-16 November 1978) with theoretical curves of constant sediment flux J overlaid. (J curves assume migration of triangular bed forms without change in shape, flux in $m^3/m/238$ days.)

to sand-wave height. The existence of a range of migration rates for each bed-form height is of course consistent with our observation of sand-wave flexing.

The lack of data points showing large migrations of the smaller bed forms, values that would correspond to the same sediment-flux curves predicted on the basis of the larger sand waves, can be explained in part by our inability to monitor these hypothetical migrations by surveys spaced months apart. That is, a sand wave 1.0-3.5 m high with a net migration distance equal to the 80+ m predicted by these curves would have migrated more than the spacing of many sand waves on the shoal, and in so doing would probably have coalesced with the next sand wave ahead, thus preventing confident crest-to-crest correlations over the eight-month study period. The general difficulty of making confident crest correlations from March to November definitely biassed this data set toward the smaller migration distances seen for these waves.

The greatest measured migration distances show a reasonable fit to the curves of constant q_s, suggesting that a long-term study of migration over a substantial part of the sand-wave field is needed for detection of these maximum potential migrations. The fit of these optimum migrations on the flood and ebb flanks of the shoal to the trend of the q_s curves suggests a larger average q_s on the northern flank than on the southern flank. However, use of Kennedy's (1969) equation to separate total sediment transport into bed-load and suspended-load components

suggests that total sediment transport may be greater on the flood flank. This result is in agreement with the qualitative arguments presented earlier to explain the morphologic differences in sand waves between the two sides of the shoal.

Average sediment transport rate associated with sand-wave migration on Middle Ground Shoal, uncorrected for porosity, seems to range between 75 and 125 $m^3/m/yr$ (Fig. 22), or when corrected for porosity, 44 and 74 $m^3/m/yr$. These values are very similar to those estimated by Jones et al. (1965), Terwindt (1971), and Bokuniewicz et al. (1977), their porosity-corrected sediment transport rates equalling 30-56 m^3/year, 31.5 m^3/year, and 54-151 m^3/year, respectively.

SCUBA diving observations documented the migration of bed forms 0.5-2.0 m high up the stoss slope of larger sand waves at average rates of about 80 m/year. A simple conversion of these migration rates to values for average sediment discharge q_s per unit width of flow (Simons et al., 1965) suggests volume transport rates, for an average megaripple height of 1.5 m, of 60.4 m^3/yr before correction for porosity. Thus, migration of megaripples (or small sand waves?) on the large sand waves seems to account for most or all of the sand transport involved in the large sand waves themselves, as should be expected if sand transport in suspension over the superimposed bed forms is unimportant. Calculated sediment transport associated with ripple migration, using migration data from Puget Sound (Kachel and Sternberg, 1971), is an order of magnitude less than needed to account for the observed sand-wave migrations. Local sus-

pended-load transport on a scale larger than ripples but smaller than megaripples must therefore contribute significantly to sand-wave migration.